The Plant Cell, Vol. 29: 2413–2432, October 2017, www.plantcell.org © 2017 ASPB.

POLYGALACTURONASE INVOLVED IN EXPANSION3 Functions in Seedling Development, Rosette Growth, and Stomatal Dynamics in *Arabidopsis thaliana*[OPEN]

Yue Rui,[a,b,1] Chaowen Xiao,[a,c,1,2] Hojae Yi,[d] Baris Kandemir,[e] James Z. Wang,[e] Virendra M. Puri,[d] and Charles T. Anderson[a,b,c,3]

[a] Department of Biology, The Pennsylvania State University, University Park, Pennsylvania 16802
[b] Intercollege Graduate Degree Program in Plant Biology, The Pennsylvania State University, University Park, Pennsylvania 16802
[c] Center for Lignocellulose Structure and Formation, The Pennsylvania State University, University Park, Pennsylvania 16802
[d] Department of Agricultural and Biological Engineering, The Pennsylvania State University, University Park, Pennsylvania 16802
[e] College of Information Sciences and Technology, The Pennsylvania State University, University Park, Pennsylvania 16802

ORCID IDs: 0000-0003-4379-4173 (J.Z.W.); 0000-0001-7481-3571 (C.T.A.)

Plant cell separation and expansion require pectin degradation by endogenous pectinases such as polygalacturonases, few of which have been functionally characterized. Stomata are a unique system to study both processes because stomatal maturation involves limited separation between sister guard cells and stomatal responses require reversible guard cell elongation and contraction. However, the molecular mechanisms for how stomatal pores form and how guard cell walls facilitate dynamic stomatal responses remain poorly understood. We characterized *POLYGALACTURONASE INVOLVED IN EXPANSION3* (*PGX3*), which is expressed in expanding tissues and guard cells. PGX3-GFP localizes to the cell wall and is enriched at sites of stomatal pore initiation in cotyledons. In seedlings, ablating or overexpressing *PGX3* affects both cotyledon shape and the spacing and pore dimensions of developing stomata. In adult plants, *PGX3* affects rosette size. Although stomata in true leaves display normal density and morphology when *PGX3* expression is altered, loss of *PGX3* prevents smooth stomatal closure, and overexpression of *PGX3* accelerates stomatal opening. These phenotypes correspond with changes in pectin molecular mass and abundance that can affect wall mechanics. Together, these results demonstrate that PGX3-mediated pectin degradation affects stomatal development in cotyledons, promotes rosette expansion, and modulates guard cell mechanics in adult plants.

INTRODUCTION

Pectins, which are major constituents of expanding cell walls in eudicots, are a group of acidic polysaccharides that includes homogalacturonan (HG), a polymer of α-1,4-linked galacturonic acid (GalA) residues; modified HGs such as xylogalacturonan and apiogalacturonan; and rhamnogalacturonan-I (RG-I) and RG-II (Atmodjo et al., 2013). HG, the predominant form of pectin in primary cell walls of *Arabidopsis thaliana* (Zablackis et al., 1995), is synthesized in a highly methylesterified form and can be demethylesterified upon delivery to the cell wall by pectin methylesterases (PMEs), generating negatively charged carboxyl groups on its GalA residues. Pectin demethylesterification can occur in continuous blocks or at random GalA residues, resulting in either wall stiffening via the formation of Ca^{2+}-cross-linked HG networks (Vincken et al., 2003) or wall loosening by means of pectin-degrading enzymes (Xiao et al., 2014). Pectin methylesterification status and molecular mass can have profound impacts on wall mechanics, affecting both cellular growth and tissue growth (Braybrook and Jönsson, 2016; Hocq et al., 2017). For example, pectin demethylesterification triggers an increase in wall elasticity during shoot meristem initiation (Peaucelle et al., 2011). In two recent studies, we reported that tissue expansion is promoted when pectin molecular mass is reduced (Xiao et al., 2017, 2014), suggesting a link between pectin size and wall stiffness in growing vegetative tissues.

Pectin-related genes, including those encoding enzymes involved in pectin biosynthesis, modification, and degradation, often exist in large families in plants (McCarthy et al., 2014). Two classes of pectin-degrading enzymes are pectate lyases (PLs), which cleave HG via β-elimination, and polygalacturonases (PGs), which hydrolyze HG backbones. In Arabidopsis, there are at least 68 annotated *PG* genes (González-Carranza et al., 2007; Kim et al., 2006; McCarthy et al., 2014). These genes display differential spatio-temporal expression patterns, which are rarely restricted to a single cell type or developmental stage (González-Carranza et al., 2007; Kim et al., 2006). Some of their gene products function in cell expansion (Xiao et al., 2017, 2014) or cell adhesion/separation (Atkinson et al., 2002; Ogawa et al., 2009; Rhee et al., 2003) in a variety of developmental contexts. However, most PGs have been neither genetically and biochemically characterized nor studied in the context of stomatal guard cells.

[1] These authors contributed equally to this work.
[2] Current address: College of Life Sciences, Sichuan University, No. 29 Wangjiang Road, Chengdu, Sichuan, China 610064.
[3] Address correspondence to cta3@psu.edu.
The author responsible for distribution of materials integral to the findings presented in this article in accordance with the policy described in the Instructions for Authors (www.plantcell.org) is: Charles T. Anderson (cta3@psu.edu).
[OPEN] Articles can be viewed without a subscription.
www.plantcell.org/cgi/doi/10.1105/tpc.17.00568

Stomatal development and function are critical for proper photosynthesis and evapotranspiration in plants. Stomatal complexes, consisting of pairs of guard cells that surround each stomatal pore and can be flanked by subsidiary cells in some plant taxa, develop from protodermal cells in the epidermis via a defined program of cell division and differentiation. The final step of this program is the division of a guard mother cell and partial separation of the cell walls of the resulting guard cells to form the stomatal pore (Bergmann and Sack, 2007; Pillitteri and Torii, 2012). Although many transcriptional regulators and signaling cascades that regulate the earlier stages of stomatal development have been characterized (Bergmann and Sack, 2007; Pillitteri and Torii, 2012), the molecular mechanisms that directly drive stomatal pore formation are currently unknown.

Mature guard cells are surrounded by strong but flexible cell walls that allow for their elastic expansion and contraction during cycles of stomatal opening and closure. These cycles can occur many thousands of times over the lifetime of a plant. In dicots, guard cell walls contain cellulose, hemicelluloses, pectins, and structural glycoproteins (Amsbury et al., 2016; Hunt et al., 2017; Majewska-Sawka et al., 2002; Rui and Anderson, 2016), and they are differentially thickened around their circumference (Zhao and Sack, 1999). Cellulose and xyloglucan function in the assembly and structural anisotropy of guard cell walls and influence stomatal opening and closure (Rui and Anderson, 2016; Woolfenden et al., 2017). However, because pectins are highly hydrated and can reversibly form cross-linked networks (Boyer, 2016), they are proposed to be major determinants of flexibility in guard cell walls (Jones et al., 2005, 2003; Shtein et al., 2017). The importance of pectins in determining the mechanical properties of guard cell walls and the dynamics of stomatal opening and closure is supported by defective stomatal opening after arabinanase treatments of epidermal peels (Jones et al., 2005, 2003), impaired stomatal functions in a *pme6* mutant (Amsbury et al., 2016), and the defective control of stomatal aperture during heat stress in a *pme34* mutant (Huang et al., 2017). However, whether and how pectins are degraded in guard cell walls by endogenous pectinases and how they might facilitate stomatal dynamics are currently unclear.

Arabidopsis transcriptome data sets for developing and mature guard cells (Bates et al., 2012; Hachez et al., 2011; Pandey et al., 2010; Yang et al., 2008) contain many pectin-related genes, providing avenues for the identification of genes responsible for generating the unique structural and mechanical properties of guard cell walls. In this work, we identified one such gene, which we named *POLYGALACTURONASE INVOLVED IN EXPANSION3* (*PGX3*). We showed that *PGX3* is expressed in a number of tissues, including guard cells. GFP-tagged PGX3 is localized in the apoplast and accumulates at sites where stomatal pores initiate in cotyledons. Phenotypic studies and biochemical characterizations in *pgx3* mutants, *PGX3* complementation, and *PGX3* overexpression plants revealed that *PGX3* promotes the irreversible expansion of growing tissues, facilitates the enlargement of developing stomatal pores in cotyledons, and maintains proper opening/closure dynamics of mature stomata in true leaves by modulating pectin size and abundance. Together, our data provide new insights into how pectin degradation is involved in the dialogues between wall biochemistry and cellular and tissue behaviors.

RESULTS

Identification and Expression Pattern of *PGX3*

To identify pectin-modifying genes that are upregulated in guard cells, we mined stomatal transcriptome data sets (Bates et al., 2012; Hachez et al., 2011; Pandey et al., 2010; Yang et al., 2008). One gene, *At1g48100*, shows ~3-fold upregulation after 4 or 48 h of induction by FAMA (Hachez et al., 2011), a basic helix-loop-helix transcription factor that promotes guard cell identity (Ohashi-Ito and Bergmann, 2006), indicating that *At1g48100* might function in guard cell differentiation. Its expression level in guard cells is 3.4-fold higher than the level in whole leaves (Bates et al., 2012) and is 42% higher in the presence of 100 μM abscisic acid (ABA) than without ABA (Yang et al., 2008). These transcriptomic data suggest that *At1g48100* might also be involved in stomatal function. *At1g48100* encodes a PG that displays enzymatic activity when heterologously expressed (Ogawa et al., 2009). Examinations of existing phylogenetic analyses of the PG family (González-Carranza et al., 2007; Kim et al., 2006; McCarthy et al., 2014) revealed that *At1g48100* is not in the same clade as previously characterized *PG* genes, including *QUARTET2* (*QRT2*) (Rhee and Somerville, 1998), *ARABIDOPSIS DEHISCENCE ZONE POLYGALACTURONASE1* (*ADPG1*) (Ogawa et al., 2009), *ADPG2* (Ogawa et al., 2009), *PGX1* (Xiao et al., 2014), and *PGX2* (Xiao et al., 2017) (Supplemental Figure 1A). Similar to those *PG* genes and many other pectin-related genes that have wide spatial-temporal expression patterns, it appears that *At1g48100* functions in both stomata and the expansion of multiple growing tissues (see below). Therefore, we named this gene *PGX3*. To specifically analyze the tissue-specific gene expression pattern of *PGX3*, we transformed a construct containing the *GUS* gene driven by the *PGX3* promoter (*ProPGX3:GUS*) into the Col background and obtained multiple independent transgenic lines that were used to determine the tissue expression pattern of *PGX3* via GUS staining (Figure 1). GUS signals were detected at the top and base of etiolated hypocotyls (Figure 1A), in roots and at lateral root initiation sites (Figures 1B to 1D), in cotyledons (Figure 1B), rosette leaves (Figure 1E), flowers (Figures 1K and 1L), siliques (Figure 1M), and seed funiculi (Figures 1N and 1O). GUS staining in epidermal peels from 3-week-old true leaves confirmed that *PGX3* is expressed in major cell types of the stomatal lineage, including meristemoids (Figure 1F), guard mother cells (Figure 1G), and both young and mature guard cells (Figures 1H to 1J). GUS signals were also present in some, but not all, pavement cells in the epidermis (Figures 1H to 1J). We quantified the expression of *PGX3* in different tissues using qPCR and found that *PGX3* is most highly expressed in flowers (Figure 1P). This is likely due to the requirement for concerted pectin degradation in the cell separation and tissue dehiscence processes occurring in this reproductive organ.

PGX3-GFP Is Localized in the Cell Wall and Accumulates at Sites of Stomatal Pore Initiation in Cotyledons

The predicted PGX3 protein contains a signal peptide/transmembrane domain and a glycosyl hydrolase 28 (GH28) domain (Supplemental Figure 1B). In the Col background, a PGX3-GFP fusion protein driven by the *PGX3* promoter (*ProPGX3:PGX3-GFP*)

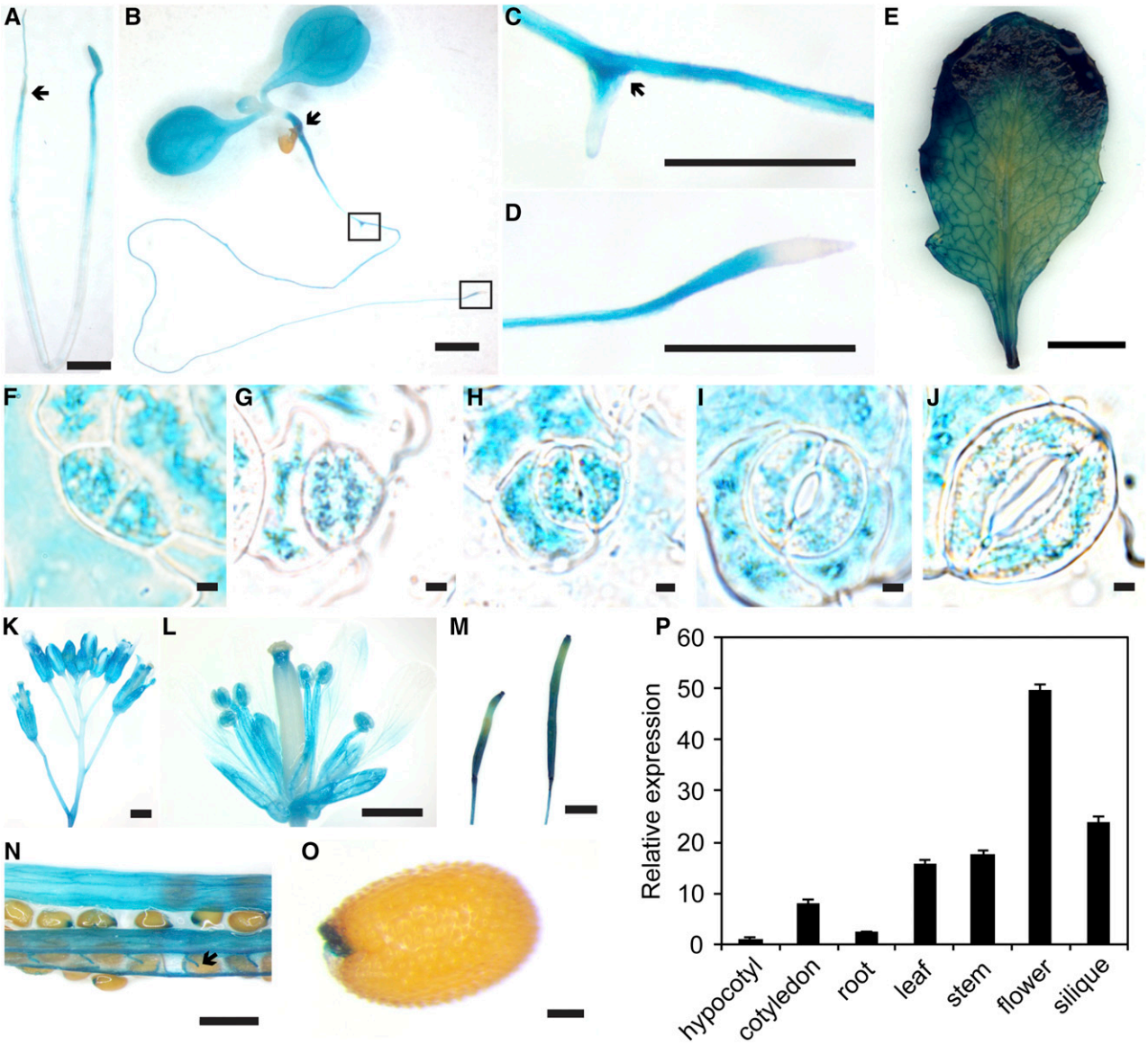

Figure 1. *PGX3* Is Expressed in Multiple Tissues and Guard Cells.

(A) to **(O)** GUS staining of *ProPGX3:GUS* transgenic plants. Images show a 6-d-old etiolated hypocotyl **(A)**, a 6-d-old light-grown seedling **(B)** with close-up views of a lateral root **(C)** and the root tip **(D)**, a 3-week-old rosette leaf **(E)**, stomatal guard cells in 3-week-old rosette leaves at different developmental stages with a meristemoid in **(F)**, a guard mother cell in **(G)**, guard cells with an initiating pore **(H)**, young guard cells **(I)**, and mature guard cells in **(J)**. Additional images show a 6-week-old inflorescence in **(K)**, a flower in **(L)**, siliques in **(M)** and **(N)**, and a mature dry seed in **(O)**. Arrows in **(A)** and **(B)** indicate collet, which is the junction between the root and the hypocotyl. Arrows indicate a lateral root initiation site in **(C)** and a funiculus in **(N)**. Bars = 1 mm in **(A)**, **(B)**, **(K)**, **(L)**, and **(N)**, 0.5 mm in **(C)** and **(D)**, 0.5 cm in **(E)**, 10 μm in **(F)** to **(J)**, 0.25 cm in **(M)**, and 100 μm in **(O)**.

(P) qPCR quantification of *PGX3* expression in different tissues. The type and age of tissues used in qPCR experiments were consistent with those in GUS staining. *ACT2* was used as an internal control, and *PGX3* expression in hypocotyls was normalized to 1. Error bars are SE and $n = 3$ biological replicates, with each biological replicate being an independent pool of tissues. For example, for 6-d-old etiolated hypocotyls, each biological replicate contained ~40 dark-grown seedlings.

was partially localized to the cell wall, as revealed by plasmolysis and imaging of PGX3-GFP in roots (Figure 2A) versus negative control roots (Figure 2B). In cotyledons of seedlings, very young stomatal complexes that had not yet initiated a stomatal pore contained PGX3-GFP distributed evenly along the border between the two guard cells. Later, during pore formation, PGX3-GFP was enriched at the site of pore initiation along with propidium iodide (PI)-stained pectins (Rounds et al., 2011) (Figure 2C). Similar results were observed when *ProPGX3:PGX3-GFP* was expressed in a *pgx3* mutant background (see below for descriptions of mutant and transgenic lines). In nontransgenic Col cotyledons, only autofluorescence from chloroplasts was evident in the GFP channel (Supplemental Figure

2A). We also used the plasma membrane marker LTI6b-GFP (Cutler et al., 2000) as another control and did not observe enrichment of LTI6b-GFP at the site of stomatal pore initiation. In fact, LTI6b-GFP was depleted at this location during pore formation (Figure 2D). In contrast with its localization in cotyledons, PGX3-GFP was not detectable in guard cells of 3-week-old true leaves (Supplemental Figure 2B), despite the fact that the *PGX3* promoter is still active as revealed by expression data (Figures 1F to 1J). The combined expression and localization data imply that *PGX3* functions in the walls of both developing and mature guard cells in both cotyledons and true leaves (see below for phenotypic characterizations).

PGX3 Functions in Seedling Development

To further analyze the functions of *PGX3*, we isolated a mutant with a T-DNA insertion in the first exon of the gene and designated it *pgx3-1* (Supplemental Figure 3A). No detectable RT-PCR product was amplified from *pgx3-1* cDNA isolated from rosette leaves using primers either flanking or downstream of the T-DNA insertion site (Supplemental Figure 3B). Two additional T-DNA insertion alleles were also isolated (Supplemental Figure 3A): *pgx3-2* has an insertion in the promoter region and was identified as a knockdown allele (Supplemental Figure 3B); *pgx3-3* has an insertion in the last exon, and the mutated gene encodes a truncated mRNA product (Supplemental Figure 3B). Because we did not observe altered growth phenotypes in either *pgx3-2* or *pgx3-3* mutants, we focused our loss-of-function analyses on the *pgx3-1* allele. Complementation analyses were performed by transforming *pgx3-1* plants with *ProPGX3:PGX3-GFP*, and 37 independent transgenic lines (*PGX3 comp*) were obtained. RT-PCR was performed on three lines in particular (*PGX3 comp* #3, #11, and #16), and expression of *PGX3* was restored in all three lines (Supplemental Figure 3C). In addition, *Pro35S:PGX3-YFP* overexpression lines (*PGX3 OE*) were generated in the Col background, and 16 independent transgenic lines were obtained. Using RT-PCR, we tested *PGX3* gene expression in six of these lines (*PGX3 OE* #1, #2, #4, #7, #12, and #16) and found that *PGX3* was overexpressed in all of these lines (Supplemental Figure 3D). *PGX3* expression was quantified in *pgx3-1*, *PGX3 comp* #3, and *PGX3 OE* #7 by qPCR, confirming that the *PGX3* expression level was significantly lower in *pgx3-1*, that it was comparable to Col controls in *PGX3 comp* #3, and that it was ~5.5-fold higher in *PGX3 OE* #7 than that in Col controls (Supplemental Figure 3E).

Given that *PGX3* expression is not limited to guard cells (Figure 1), we compared seed germination of wild-type controls and *PGX3* genotypes, as germination can affect seedling growth. We monitored seed germination following stratification at 0.5-d intervals up to 2.5 d under dark-grown or light-grown conditions and found that germination in *PGX3 comp* #3 and *PGX3 OE* #7 transgenic lines was accelerated during the first 1.5 d compared with Col controls or *pgx3-1* mutants (Supplemental Figures 4A and 4B). On day 2.5 after stratification, the germination percentage was comparable among Col, *PGX3 comp* #3, and *PGX3 OE #7* and was slightly lower in *pgx3-1* mutants (Supplemental Figures 4A and 4B).

We next analyzed *PGX3* function in the context of seedling development. In etiolated seedlings, *pgx3-1* hypocotyls were shorter than in Col controls. *PGX3 comp* #3 hypocotyls started out longer but ended up shorter than Col controls, and *PGX3 OE* #7 hypocotyls were longer than Col controls only on days 2 and 3 following stratification (Supplemental Figure 4C). Light-grown *pgx3-1* seedlings displayed slower root growth than Col controls (Figure 3A), whereas *PGX3 comp* #3 and *PGX3 OE* #7 seedling roots were slightly but significantly longer than Col controls but without any significant changes in growth rate (Supplemental Figure 4D). These growth patterns were also seen in some of the additional transgenic lines that we generated: Both etiolated hypocotyl length and root growth were enhanced in *PGX3 OE* #2 seedlings (Supplemental Figures 5A and 5B). Interestingly, in light-grown *pgx3-1* seedlings, cotyledon shape was also disrupted. Whereas a majority of Col control cotyledons were convex, concave cotyledons were much more frequent in *pgx3-1* mutants (Figures 3B and 3C). In contrast, cotyledon shape was not altered by *PGX3* overexpression, as convex cotyledons were observed in 96% of *PGX3 OE* #7 seedlings (68 out of 71 seedlings). Together, these data indicate that *PGX3* functions in multiple developmental processes in seedlings, including root and hypocotyl elongation and the regulation of cotyledon shape.

Ablation of *PGX3* Affects Stomatal Clustering and Results in Smaller Pores in the Developing Stomata of Cotyledons

Given that *PGX3* expression is upregulated by experimental induction of guard cell differentiation (Hachez et al., 2011) and that in seedlings, PGX3-GFP is enriched at stomatal pore initiation sites in young guard cells in cotyledons (Figure 2C), we assessed stomatal development in relation to *PGX3* ablation or overexpression in the cotyledons of 6-d-old light-grown seedlings (Figures 3D to 3J). We observed more clustered stomatal complexes that violate the one-cell spacing rule (Bergmann and Sack, 2007; Pillitteri and Torii, 2012) in *pgx3-1* cotyledons than in Col controls (Figures 3D and 3E). In single stomatal complexes that were not part of stomatal clusters, stomatal pore length, pore width, guard cell pair height, and the ratio of pore length to guard cell pair height were all significantly smaller in *pgx3-1* mutant cotyledons than in Col controls (Figures 3F to 3J). In *PGX3 comp* #3 seedlings, stomatal pore length and pore length:guard cell pair height were smaller than in Col controls, but larger than in *pgx3-1* mutants, and pore width and guard cell pair height did not differ from Col controls (Figures 3F to 3J). In *PGX3 OE* #7 seedlings, stomatal pore length and pore length:guard cell pair height were larger than in Col controls, whereas stomatal pore width and guard cell pair height did not differ from Col controls (Figures 3F to 3J). Thus, in seedling cotyledons, *PGX3* influences stomatal pore dimensions and increases pore length and pore length:guard cell pair height ratios.

In Adult Plants, *PGX3* Is Required for Rosette Expansion, but Does Not Affect Stomatal Density or Size in True Leaves

Because *PGX3* is expressed not only in seedlings but also in adult plants (Figure 1), we next focused our phenotypic characterizations on adult tissues. In adult plant cohorts grown together with separate sets of Col controls for each *PGX3* genotype, rosette canopy area was smaller in *pgx3-1* plants than in Col controls, *PGX3 comp* #3 rosette areas did not differ from Col controls, and

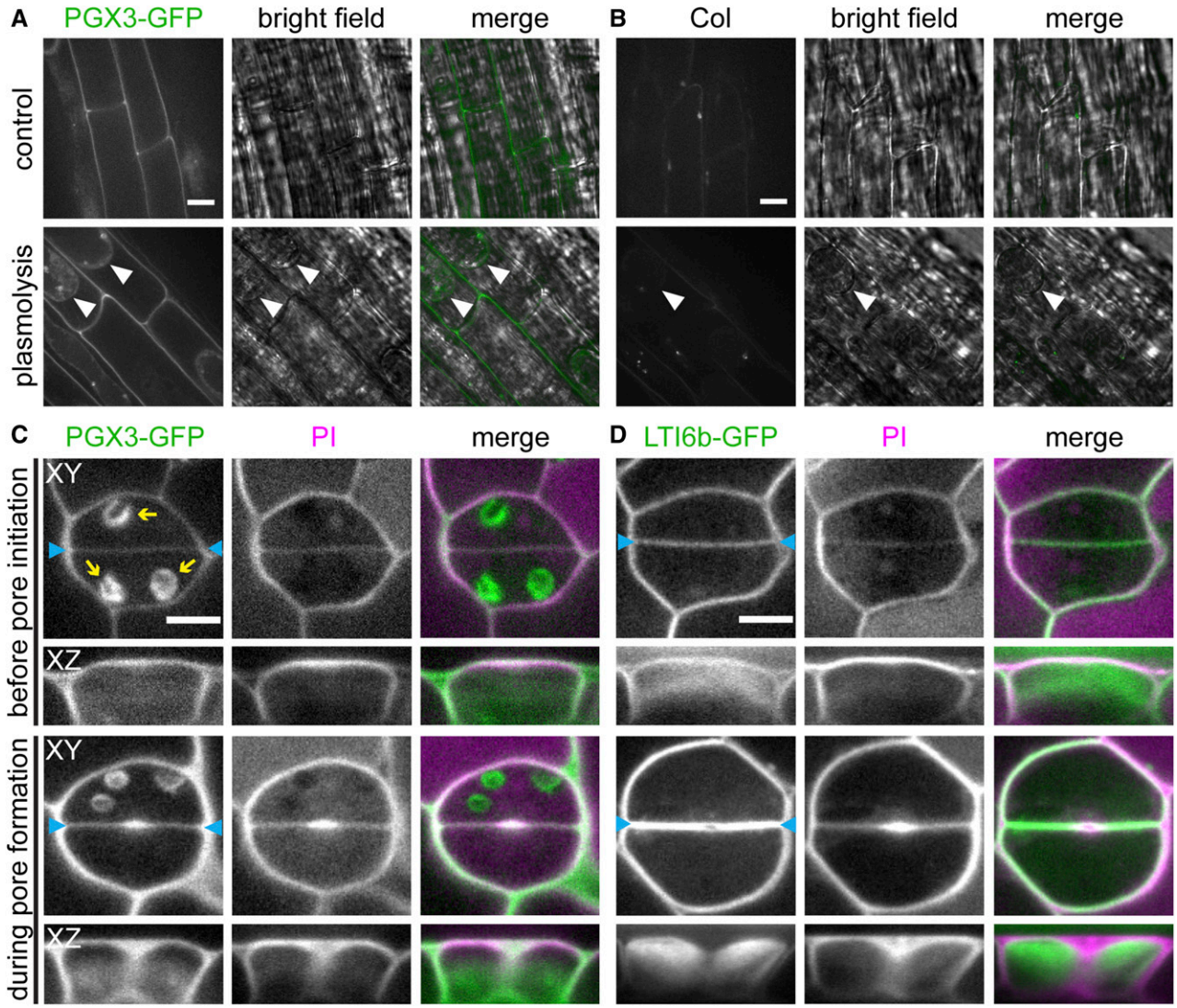

Figure 2. In Seedlings, PGX3-GFP Is Localized in the Cell Wall and Accumulates at Stomatal Pore Initiation Sites.

(A) and **(B)** Fluorescence and bright-field images of 5-d-old roots. Images show roots expressing *ProPGX3:PGX3-GFP* **(A)** or Col roots **(B)** under the control condition (top panel) or plasmolyzed with 1 M mannitol for 5 min (bottom panel). White arrowheads indicate membranes separated from the cell wall.
(C) and **(D)** PI staining in developing guard cells of 4-d-old seedlings. Images show seedlings expressing *ProPGX3:PGX3-GFP* **(C)** or a membrane marker, GFP-tagged LTI6b **(D)**. Blue arrowheads indicate cell plates between sister guard cells. Yellow arrows indicate autofluorescence from chloroplasts. XY and XZ indicate projections in the XY and XZ directions, respectively.
Bars = 10 μm in **(A)** and **(B)** and 5 μm in **(C)** and **(D)**.

PGX3 OE #7 rosettes were larger than Col controls (Figures 4A and 4B). These growth trends were also observed in some of the additional transgenic lines that we generated: Rosette area in *PGX3 comp* #11 plants was not significantly different from side-by-side Col controls (Supplemental Figures 6A and 6B), whereas rosette area was enhanced in *PGX3 OE* #2 plants (Supplemental Figures 6C and 6D). In contrast to other Arabidopsis PG mutants (Ogawa et al., 2009; Xiao et al., 2017, 2014), defects in stem growth, floral development, and floral organ abscission were not evident in *pgx3-1* adult plants.

To investigate whether altered pore size in the stomata of cotyledons also occurs in the stomata of true leaves in adult plants, we monitored stomatal complex size, stomatal density, stomatal index, and pavement cell size across 4 weeks of development in true leaves of Col, *pgx3-1*, *PGX3 comp* #3, and *PGX3 OE* #7 plants. Clear trends of genotype-dependent, statistically significant differences were not observed for any of the parameters tested (Figures 4C to 4F), although pavement cell size was slightly bigger or smaller when *PGX3* is overexpressed or absent in 1- to 3-week-old true leaves (Figure 4F). Taken together, these data suggest that *PGX3* is required for rosette leaf growth and that, unlike in cotyledons, stomatal complex size in true leaves does not correlate with *PGX3* expression, possibly due to the expression of additional *PG* genes in true leaves.

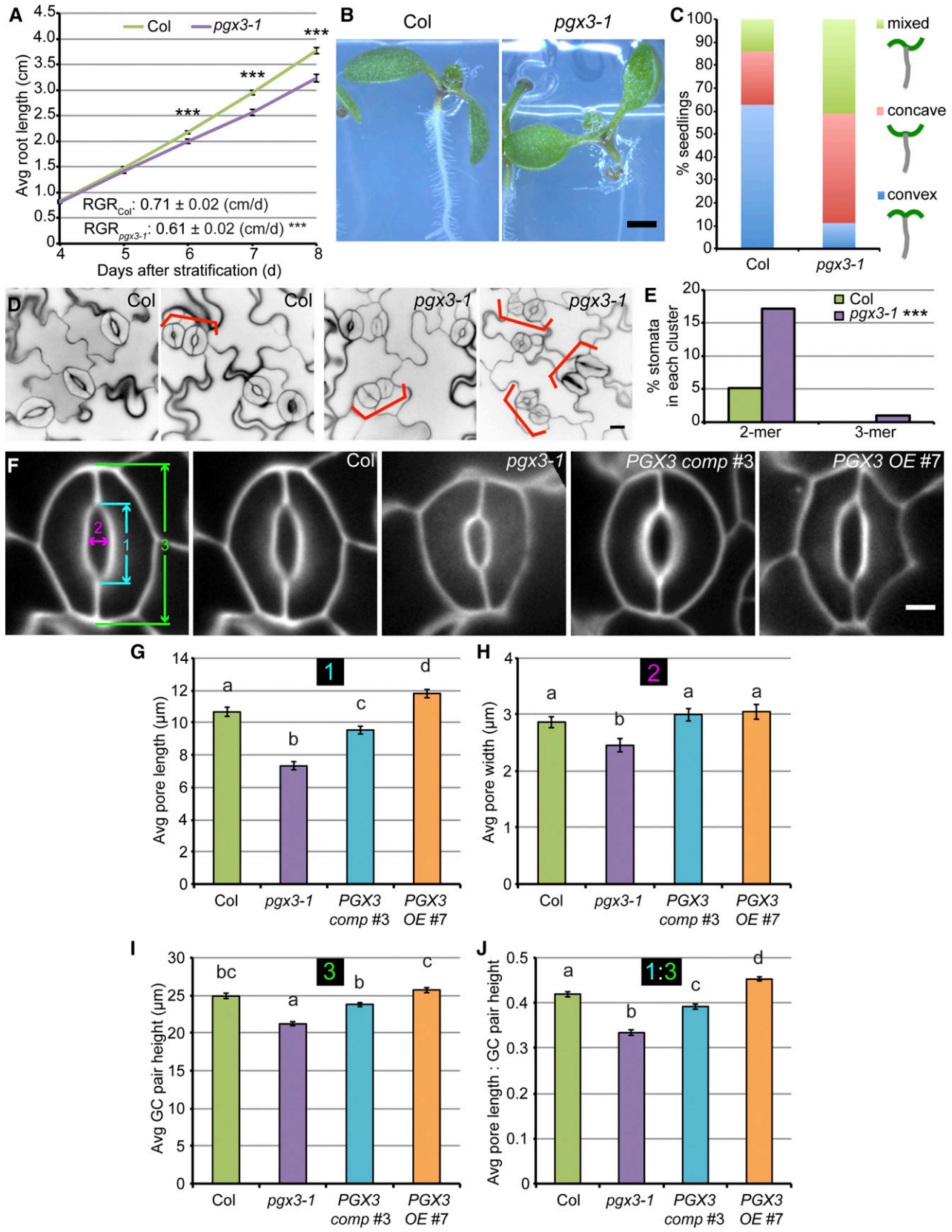

Figure 3. In Seedlings, *PGX3* Functions in Root Elongation and Regulates Cotyledon Shape, Stomatal Spacing, and Stomatal Pore Size.

(A) Primary root length of 4- to 8-d-old light-grown seedlings in Col and *pgx3-1*. Error bars are SE ($n \geq 91$ seedlings per genotype per day from three independent experiments; ***P < 0.001, Student's *t* test). Relative growth rates (RGRs) of roots in each genotype are indicated in the graph.

Stomatal Dynamics in True Leaves Are Asymmetrically Altered by Changes in *PGX3* Expression

The fact that *PGX3* expression in mature guard cells is higher than that in whole leaves (Bates et al., 2012) led us to investigate stomatal function in more detail in adult plants. To test the effects of *PGX3* on mature stomatal complexes, stomatal responses were assessed in rosette leaves from 3- to 4-week-old Col, *pgx3-1*, *PGX3 comp* #3, and *PGX3 OE* #7 plants using fusicoccin (FC) or light to induce stomatal opening, and using abscisic acid (ABA) or darkness to induce stomatal closure. In experiments where excised true leaves were treated with FC or ABA and stomatal pore widths were measured from epidermal peels of these leaves at 30-min intervals up to 150 min (Figures 5A and 5B), *pgx3-1* stomata opened similarly to Col controls in response to FC (Figure 5A). However, in response to ABA, average pore widths in *pgx3-1* leaves deviated significantly from Col controls at 30-, 60-, 120-, and 150-min time points, with average pore widths being smaller at 30 min, but larger at 60, 120, and 150 min (Figure 5B). Overall, this resulted in a stepwise closure pattern for populations of *pgx3-1* stomata. In *PGX3 comp* #3 leaves, stomatal responses to FC and ABA were similar to Col controls (Figures 5A and 5B). *PGX3 OE* #7 stomata, in contrast, initially opened more rapidly in response to FC, but their average pore widths did not differ from Col controls after 150 min of FC exposure (Figure 5A). However, *PGX3 OE* #7 stomata closed similarly to Col controls in response to ABA (Figure 5B).

To analyze the dynamics of stomatal closure in individual stomata with higher temporal resolution, stomatal closure was induced by applying ABA to Col, *pgx3-1*, and *PGX3 OE* #7 epidermal peels mounted in microscope chambers, and then the same cells were imaged every 10 min (Supplemental Movie 1). In these experiments with epidermal peels, stomatal closure kinetics were more variable in all three genotypes (Figure 5C) than in the whole-leaf experiments described above (Figure 5B). However, median pore widths in Col and *PGX3 OE* #7 epidermal peels still decreased from ~3 μm at 0 min to ~1 μm at 150 min, whereas in *pgx3-1* epidermal peels, median pore widths only diminished from 3.1 μm at 0 min to 2.2 μm at 150 min (Figure 5C). This again indicated that *pgx3-1* guard cells are defective in stomatal closure. Fluctuations in pore width (opening then closure, or closure then opening) during the time courses were also observed in *pgx3-1* stomata, but not in Col or *PGX3 OE* #7 stomata (Figure 5D; Supplemental Movie 1).

In addition to FC and ABA, we also used light or darkness to induce stomatal opening or closure. Stomatal pore widths were measured every 30 min after excised true leaves of *pgx3-1* were placed in darkness, and we found that the closure pattern was more stepwise than for Col control stomata (Supplemental Figure 7A). When excised leaves of *PGX3 OE* #7 were placed in the light, stomatal opening was initially faster than for Col controls (Supplemental Figure 7B), consistent with stomatal responses to FC (Figure 5A). To further investigate stomatal opening dynamics in individual stomata, Col and *PGX3 OE* #7 epidermal peels mounted in microscope chambers were illuminated and the same stomata were imaged every 10 min thereafter (Supplemental Movie 2). In these experiments using epidermal peels, stomata opened to a lesser degree in both genotypes (Supplemental Figures 7C and 7D) than in the aforementioned experiments using excised leaves (Supplemental Figure 7B). This was possibly due to the fact that epidermal peels were sandwiched between a slide and a cover slip and this perturbation could affect stomatal responses. As a result, median stomatal pore widths in Col controls increased only from 0.3 μm at 0 min to 0.4 μm at 150 min, whereas median pore widths in *PGX3 OE* #7 were 0.3 μm at 0 min, but increased to 1.1 μm at 150 min (Supplemental Figure 7C), suggesting that stomata open more readily when *PGX3* is overexpressed.

PGX3 expression did not influence stomatal complex size in true leaves during 4 weeks of development (Figure 4E). To further test whether altered stomatal dynamics in adult leaves (Figure 5; Supplemental Figure 7 and Supplemental Movies 1 and 2) was due to changes in stomatal dimensions, we measured stomatal pore length, guard cell pair height, guard cell pair width, guard cell length, and guard cell diameter (Rui and Anderson, 2016), in addition to stomatal pore width, for all genotypes and confirmed that stomata in true leaves of 3-week-old Col, *pgx3-1*, and *PGX3 OE* #7 plants were similar in size (Supplemental Tables 1 and 2). Together, data from the above experiments and measurements suggest that pectin degradation by PGX3 modulates stomatal dynamics asymmetrically. In the absence of *PGX3*, the smooth compression of guard cell walls during stomatal closure is impaired, whereas excess pectin degradation caused by *PGX3* overexpression might accelerate wall expansion during stomatal opening.

PGX3 Modulates Demethylesterified HG Abundance in Guard Cells in True Leaves

To investigate the mechanism by which *PGX3* regulates stomatal dynamics, we tested whether changes in *PGX3* expression could

Figure 3. (continued).

(B) and **(C)** Cotyledon shape of 6-d-old *pgx3-1* mutants. Panels show representative images **(B)** and quantifications **(C)** ($n \geq 107$ seedlings per genotype from three independent experiments).

(D) and **(E)** Stomatal cluster analysis in cotyledons of 6-d-old Col and *pgx3-1* seedlings. Panels show representative PI staining **(D)** and quantifications **(E)** ($n \geq 271$ stomata from 12 seedlings per genotype, two independent experiments; ***$P < 0.001$, χ^2 test). Red brackets in **(D)** indicate clustered stomata.

(F) Stomatal dimensions. Shown are brackets representing pore length (1, blue), pore width (2, magenta), and guard cell pair height (3, green) along with representative PI staining images of stomata in 6-d-old seedlings of Col, *pgx3-1*, *PGX3 comp* #3, and *PGX3 OE* #7.

(G) to **(J)** Measurements of pore length **(G)**, pore width **(H)**, guard cell pair height **(I)**, and the ratio of pore length to guard cell pair height **(J)** in 6-d-old Col, *pgx3-1*, *PGX3 comp* #3, and *PGX3 OE* #7 seedlings. Numbers in black boxes on the graphs correspond to numbers in stomatal dimension legend in **(F)**. Error bars are SE, and lowercase letters represent significantly different groups ($n \geq 140$ stomata from at least 10 seedlings per genotype, two independent experiments; $P < 0.05$, one-way ANOVA and Tukey test).

Bars = 1 mm in **(B)**, 10 μm in **(D)**, and 5 μm in **(F)**.

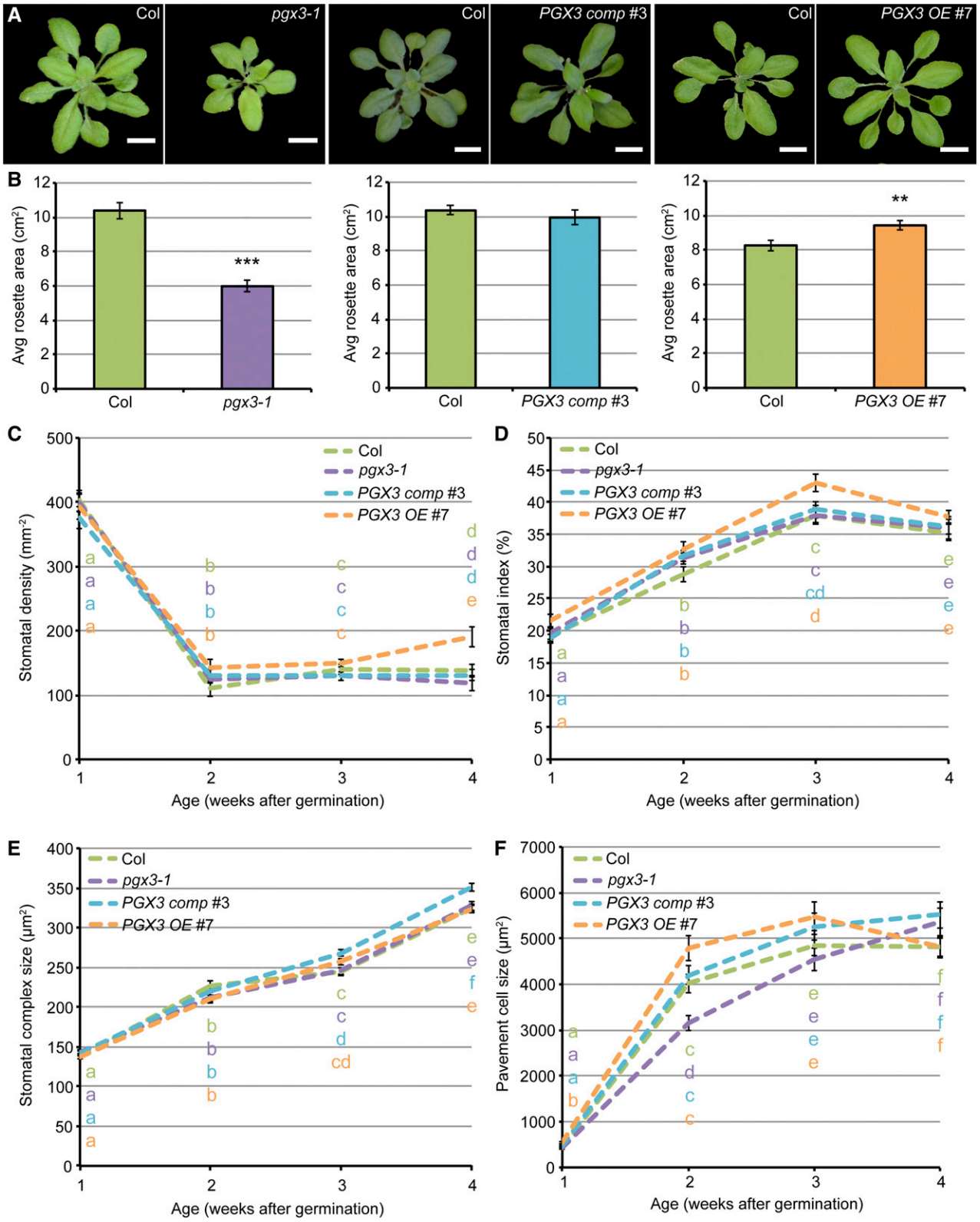

Figure 4. *PGX3* Is Required for Rosette Expansion, but Does Not Affect Stomatal Density or Size in True Leaves.

have specific architectural or compositional effects on guard cell walls. Because cellulose is a major structural component of cell walls in growing eudicot tissues and is proposed to interact with pectins (Cosgrove, 2014), we investigated whether cellulose organization differs in *pgx3-1* guard cells relative to Col controls. Using the cellulose dye Pontamine Fast Scarlet 4B (Anderson et al., 2010) to label stomata that had been induced to open or close by treatment with FC or ABA, we observed similar labeling patterns and changes in cellulose anisotropy (Rui and Anderson, 2016) in both genotypes (Supplemental Figures 8A and 8B), indicating that cellulose organization was more diffuse in guard cells surrounding open stomata but was more fibrillar in guard cells surrounding closed stomata in both Col controls and *pgx3-1* mutants. To probe HG abundance and distribution in guard cells as a function of *PGX3* expression, we applied either a chitosan-oligosaccharide-Alexa 488 probe, COS^{488}, which binds to negatively charged carboxyl groups on stretches of demethylesterified GalA residues in HG (Mravec et al., 2014), or propidium iodide, which binds to single demethylesterified GalA residues (Rounds et al., 2011) (Figure 6). These probes were used prior to immunolabeling because the latter method is not compatible with imaging of intact cells, whereas the cuticle permeability of these small molecular probes enabled labeling of intact guard cells without fixation or sectioning, allowing for quantitative analyses of labeling intensity in three dimensions. COS^{488}-labeled the walls of guard cells, with more fluorescence at guard cell junctions (Figure 6A). Quantifying COS^{488} labeling intensity in individual cells (Supplemental Figure 8C) revealed that labeling in *pgx3-1* cells was slightly more intense than in Col controls (Figures 6A and 6B), implying that more COS^{488} binding sites are present in *pgx3-1* guard cell walls. PI labeling was likewise more intense in regions of *pgx3-1* cells that excluded autofluorescent phenolic-containing ridges (Supplemental Figure 8C) than in Col controls (Figures 6C and 6D), again indicating higher levels of demethylesterified HG in *pgx3-1* mutant walls. COS^{488} and PI labeling in *PGX3 comp* #3 guard cells did not differ from Col controls (Figure 6), but in *PGX3 OE* #7 guard cells, both COS^{488} and PI labeling were less intense than in Col controls (Figure 6). This implied that demethylesterified HG levels were reduced in *PGX3 OE* #7 guard cells. In neighboring pavement cells, COS^{488} labeling was slightly lower in *PGX3 OE* #7 leaves (Supplemental Figure 8D), but PI labeling did not differ by genotype (Supplemental Figure 8E).

To further validate the results from labeling with small molecule dyes, we also performed immunolabeling in cross sections of rosette leaves of 3- to 4-week-old Col, *pgx3-1*, and *PGX3 OE* #7 plants using representative antibodies that recognize different forms of HG (Figure 7; Supplemental Figures 9 to 11): LM19, which recognizes demethylesterified HG (Verhertbruggen et al., 2009); LM20, which recognizes methylesterified HG (Verhertbruggen et al., 2009); 2F4, which recognizes Ca^{2+}-cross-linked HG (Liners et al., 1989); and JIM7, which recognizes methylesterified HG with a methylesterification degree of 15 to 80% (Knox et al., 1990; Willats et al., 2000). Compared with control sections that were not incubated with primary antibodies (Supplemental Figures 9 and 11), LM20 and JIM7 displayed more uniform labeling patterns relative to the other two antibodies (Figure 7B; Supplemental Figure 11A), whereas 2F4 labeling was the most punctate (Figure 7C) among all four antibodies tested.

To quantify differences in immunolabeling, we recorded the raw integrated density of secondary antibody-associated fluorescence for every section and the corresponding guard cell wall area as outlined by S4B costaining, subtracted background autofluorescence as measured in control sections, and calculated the background-corrected intensity per area as an estimate of antibody labeling intensity (Supplemental Figures 10 and 11C). Compared with Col controls, *pgx3-1* mutant guard cells had stronger labeling for all four antibodies (Figure 7; Supplemental Figures 10 and 11), whereas in *PGX3 OE* #7 guard cells, LM19 and 2F4 binding appeared to be weaker (Figures 7A and 7C; Supplemental Figures 10A and 10C), but LM20 and JIM7 signals seemed to be brighter (Figure 7B; Supplemental Figures 10B and 11). Although 2F4 displayed the weakest labeling among all four antibodies tested for every genotype, its punctate labeling intensity was above background levels (Figure 7C; Supplemental Figure 9C; see also the magnitude of AFU in Supplemental Figure 10C). The immunolabeling data for LM19 agree with our dye labeling results described above, confirming that demethylesterified HG is more abundant in *pgx3-1* guard cell walls, but is less abundant when *PGX3* is overexpressed. Together, these pectin labeling results indicate that *PGX3* fine tunes the level of demethylesterified HG in guard cell walls, providing a molecular explanation for the altered stomatal dynamics observed in *PGX3* knockout and overexpression plants.

PGX3 Overexpression Increases Total PG Activity and Reduces HG Molecular Mass

PGX3 degrades HG when expressed heterologously (Ogawa et al., 2009), but its in vivo activity has not been reported. Therefore, we assayed total PG activity and pectin molecular mass in Col, *pgx3-1*, and *PGX3 OE* #7 tissues (Figure 8). In protein extracts from Col, *pgx3-1*, and *PGX3 OE* #7 flowers, where *PGX3* is most highly expressed (Figure 1P), total PG activity was substantially higher in *PGX3 OE* #7 samples than in Col controls (Figure 8A). To analyze the effects of *PGX3* expression on pectin molecular mass, we used size-exclusion chromatography to

Figure 4. (continued).

(A) and **(B)** Representative segmented images of rosettes **(A)** and measurements of rosette area **(B)** in 3-week-old Col, *pgx3-1*, *PGX3 comp* #3, and *PGX3 OE* #7 plants. Bars = 1 cm in **(A)**. Error bars are SE in **(B)** ($n \geq 46$ plants per genotype from three independent experiments; $^{**}P < 0.01$ and $^{***}P < 0.001$, Student's *t* test). Note that side-by-side controls were always used for each genotype in every independent experiment.

(C) to **(F)** Stomatal density **(C)**, stomatal index **(D)**, stomatal complex size **(E)**, and pavement cell size **(F)** in 1-, 2-, 3-, and 4-week-old true leaves of Col, *pgx3-1*, *PGX3 comp* #3, and *PGX3 OE* #7 plants. Error bars are SE. Lowercase letters represent significantly different groups and colors of the letters correspond to the colors of genotypes. For **(C)** and **(D)**, $n \geq 3$ fields of view from six individual plants per genotype. For **(E)**, $n \geq 55$ stomatal complexes from six individual plants per genotype. For **(F)**, $n \geq 71$ pavement cells from six individual plants per genotype. $P < 0.05$, one-way ANOVA and Tukey test.

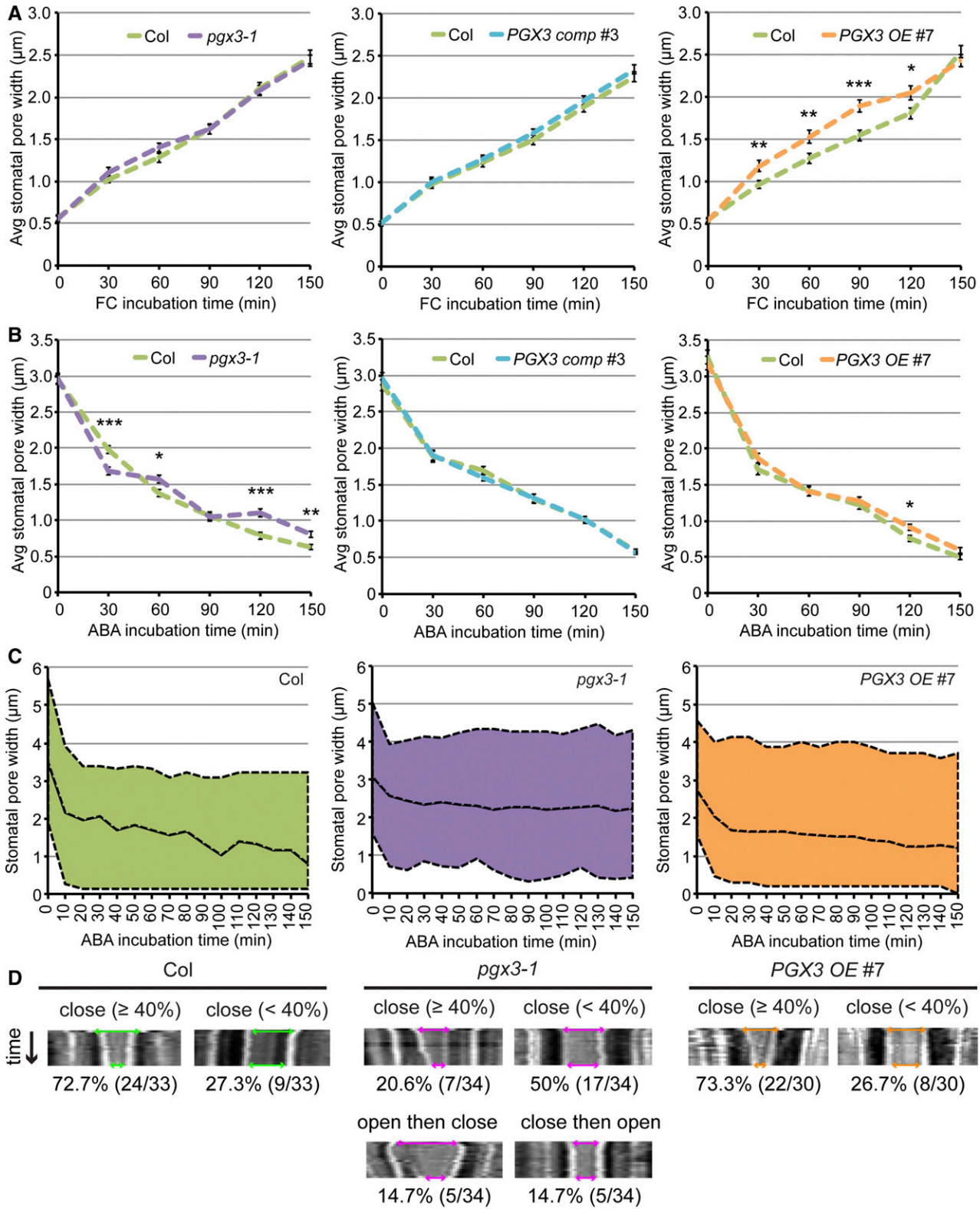

Figure 5. *PGX3* Modulates Stomatal Dynamics in Adult Plants.

(A) and **(B)** Average stomatal response to 1 μM FC-induced opening **(A)** or 50 μM ABA-induced closure **(B)** on the population level in 3- to 4-week-old Col, *pgx3-1*, *PGX3 comp* #3, and *PGX3 OE* #7 plants. Error bars are SE ($n \geq 94$ stomata per genotype per time point from three independent experiments; *P < 0.05, **P < 0.01, and ***P < 0.001, Student's *t* test).

(C) and **(D)** Individual stomatal dynamics in 3- to 4-week-old Col controls, *pgx3-1* mutants, and *PGX3 OE* #7 plants during 50 μM ABA-induced closure ($n \geq$ 30 stomata per genotype from at least four independent experiments). For each graph in **(C)**, top, middle, and bottom lines correspond to the maximum,

assay HG extracted from Col, *pgx3-1*, and *PGX3 OE* #7 leaves, where stomata are present and sufficient pectins could be recovered for measurement. Both average HG molecular mass as estimated by the elution fraction number corresponding to major peaks and total extracted HG amounts as estimated by the area under the absorbance curve for extracted uronic acids were lower in *PGX3 OE* #7 leaves than in Col controls. By contrast, HG size was only subtly different in *pgx3-1* leaves, but total extractable HG was higher (Figure 8B). These results are consistent with the aforementioned HG abundance data in guard cells from our labeling experiments (Figures 6 and 7) and provide in vivo evidence that PGX3 is a polygalacturonase that degrades pectins in the walls.

DISCUSSION

In this work, we analyzed guard cell-specific transcriptomes (Bates et al., 2012; Hachez et al., 2011; Pandey et al., 2010; Yang et al., 2008) to guide reverse genetics experiments that would identify and characterize genes that function in the guard cell wall to regulate stomatal dynamics. Given that the expression of most cell wall-related genes is not limited to a single cell type, this tandem strategy can also reveal gene functions in many other aspects of plant growth and development. *PGX3* is one such gene that is upregulated when induced by FAMA (Hachez et al., 2011) and is expressed in mature guard cells (Bates et al., 2012; Yang et al., 2008). In our study, we expanded the functional repertoire of PGs by providing genetic, cytological, and biochemical evidence that, in additional to its requirement for irreversible tissue expansion in seedlings and adult rosettes, PGX3 is a PG that fine-tunes HG abundance and molecular mass in guard cell walls to maintain their flexibility during stomatal dynamics.

PGs comprise a large family, which has 68 members in Arabidopsis (González-Carranza et al., 2007; Kim et al., 2006; McCarthy et al., 2014). As a result of potential redundancy within the PG family, phenotypes of loss-of-function mutants for a single *PG* gene can be masked by other *PG* genes. Therefore, it was surprising to us that *pgx3-1* mutants exhibited growth phenotypes in multiple tissues and at different developmental stages (Figures 3 and 4; Supplemental Figures 4 to 6), some of which were subtle but statistically significant. The results that total PG activity and pectin size remained largely unaltered in *pgx3-1* mutants compared with Col controls (Figure 8) might also be due to functional redundancy. PGs degrade pectins in a variety of developmental contexts (Ogawa et al., 2009; Rhee et al., 2003; Xiao et al., 2017, 2014), but relatively few plant PGs have been biochemically characterized, and the functions of many *PG* genes remain undefined.

Of the PGs characterized in Arabidopsis, PGX1 functions in cell expansion and floral organ patterning (Xiao et al., 2014), PGX2 promotes cell expansion and influences stem bolting and lignification (Xiao et al., 2017), QRT2 and QRT3 are required for microspore separation (Rhee et al., 2003; Rhee and Somerville, 1998), and ADPG1 and ADPG2 are essential for silique dehiscence and contribute to floral organ abscission (Ogawa et al., 2009). Phylogenetic analyses of PGs in Arabidopsis reveal that PGX3 is not closely related to any of the previously published Arabidopsis PGs (Supplemental Figure 1A) (Kim et al., 2006; McCarthy et al., 2014). When expressed in *Escherichia coli* and purified, the PG activity of PGX3 is higher than the activities of ADPG1, ADPG2 (Ogawa et al., 2009), or PGX2 (Xiao et al., 2017), but lower than the reported activity of PGX1 (Xiao et al., 2014). However, given the potential for protein inactivation and/or inhibition during heterologous expression and purification, more direct comparisons of PG activity are required to clearly define the relative activities of these and other Arabidopsis PGs in vivo. In addition, differences in substrate affinity, catalytic activity, processivity, autoinhibition, and/or pH sensitivity might be responsible for these results, but these factors have not been fully defined for plant PGs. Nonetheless, our biochemical and functional characterizations of PGX3 have revealed a unique PG that regulates seedling root growth, cotyledon shape, stomatal development in cotyledons, rosette expansion, and stomatal dynamics in true leaves. The fact that none of the aforementioned *PG* genes is expressed in a single tissue or cell type suggests that PGs play overlapping yet diverse roles during plant growth and development.

Similar to PGX1 (Xiao et al., 2014) and PGX2 (Xiao et al., 2017), PGX3 regulates seedling growth (Figure 3A; Supplemental Figures 4 and 5) and rosette expansion in adult plants (Figures 4A and 4B; Supplemental Figure 6). But different from the two previously characterized *PGX* genes, *PGX3* also has a function in seed germination (Supplemental Figures 4A and 4B). The effect of seed germination on seedling development, together with the function of *PGX3* in tissue growth (see relative growth rates in Figure 3A; Supplemental Figures 4D and 5B), contributes to the determination of etiolated hypocotyl length and root length in young seedlings. In adult plants, we conclude that the altered rosette size when *PGX3* is absent or overexpressed (Figures 4A and 4B) is mainly due to changes in pavement cell size (Figure 4F), but not stomatal density, morphology, or size (Figures 4C to 4E; Supplemental Tables 1 and 2). Although *PGX3* expression is roughly correlated with changes in pavement cell size (Figure 4F), *ProPGX3:GUS* was not detected in all pavement cells in the leaf epidermis (Figures 1H to 1J). The fact that *PGX3* is expressed in both guard cells and pavement cells (Figures 1F to 1J) does not preclude the conclusion that the stomatal phenotypes we observed (Figures 5 to 7) in adult leaves of *pgx3-1* and *PGX3 OE #7* plants are a result of changes in *PGX3* expression in guard cells, although indirect interactions between pectin status in pavement cells and guard cells are possible.

Stomatal development involves several rounds of cell fate transitions and guard cell specification, and this process has been well established by the identification of many regulating factors (reviewed in Bergmann and Sack, 2007; Pillitteri and Torii, 2012).

Figure 5. (continued).

median, and minimum stomatal pore width values at each time point, respectively. Kymographs with quantifications in **(D)** were generated from the same set of images in Supplemental Movie 1. Double-headed arrows in each kymograph indicate stomatal pore width at the beginning or the end of ABA-induced closure.

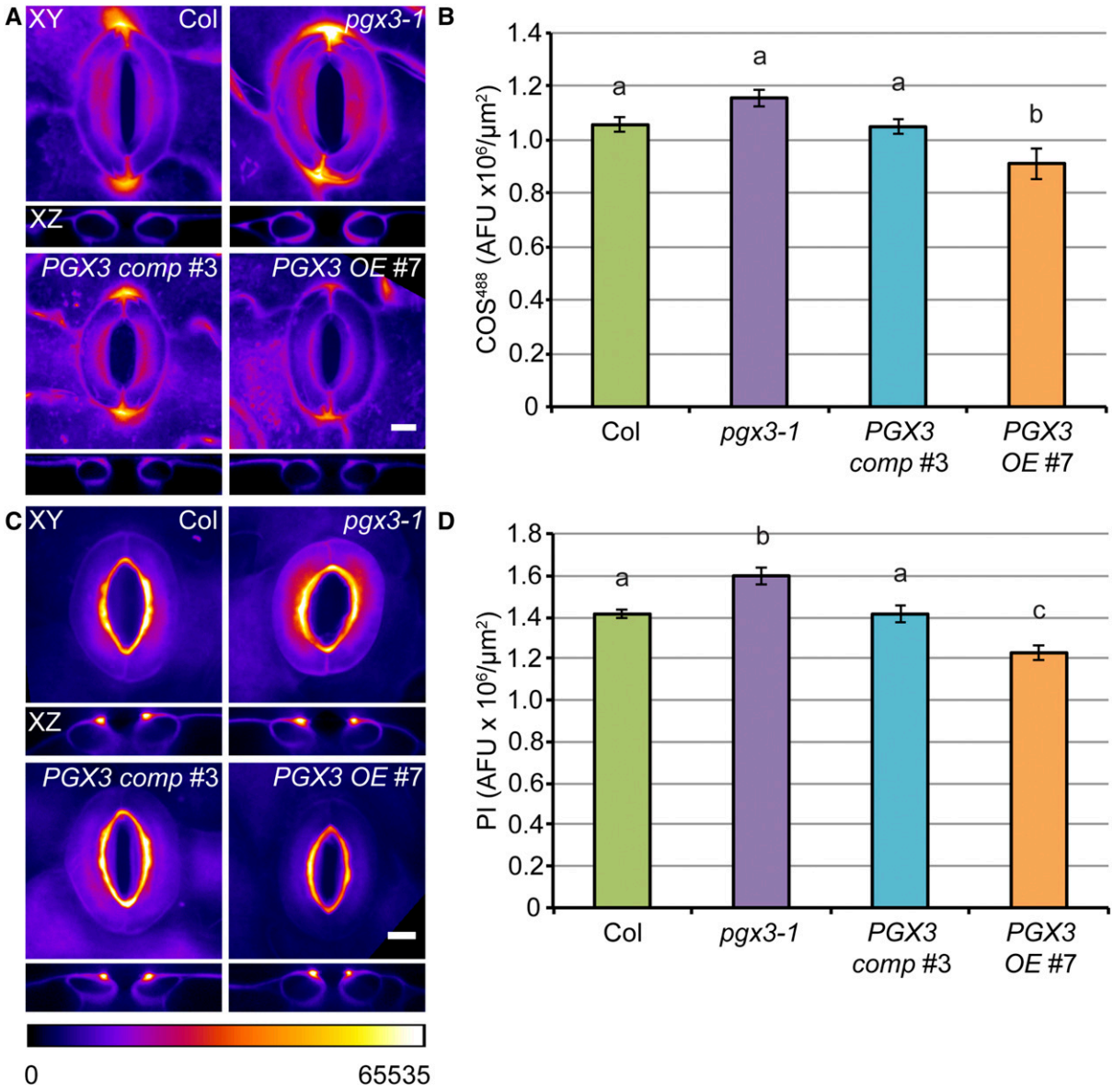

Figure 6. *PGX3* Regulates the Level of Demethylesterified HG in Guard Cells in True Leaves.

(A) and **(B)** COS^{488} labeling in guard cells. Images show representative XY and XZ maximum projection images **(A)** and fluorescence intensity **(B)** quantified in the walls of individual guard cells in 3- to 4-week-old Col, *pgx3-1*, *PGX3 comp* #3, and *PGX3 OE* #7 plants. Error bars are SE, and lowercase letters represent significantly different groups ($n \geq 42$ guard cell pairs from six plants per genotype, two independent experiments; $P < 0.05$, one-way ANOVA and Tukey test). **(C)** and **(D)** PI staining in guard cells. Images show representative XY and XZ maximum projection images **(C)** and fluorescence intensity **(D)** quantified in the walls of individual guard cells in 3- to 4-week-old Col, *pgx3-1*, *PGX3 comp* #3, and *PGX3 OE* #7 plants. Error bars are SE, and lowercase letters represent significantly different groups ($n \geq 36$ guard cell pairs from six plants per genotype, two independent experiments; $P < 0.05$, one-way ANOVA and Tukey test). Images in **(A)** and **(C)** were applied with a fire look-up table to facilitate the comparison of fluorescence intensity. XZ projections in **(A)** and **(C)** were made from the midline in the Y direction. Bars = 5 μm in **(A)** and **(C)**.

However, the mechanisms underlying pore formation, the final step of stomatal development that requires controlled separation between sister guard cell walls (Bergmann and Sack, 2007), have remained largely unexplored. The enrichment of PGX3-GFP at sites of stomatal pore initiation (Figure 2C) and the observation that varying *PGX3* expression differentially altered stomatal pore size in cotyledons (Figures 3F to 3J) indicate the importance of this gene in stomatal pore formation in cotyledons. However, because stomatal pores still developed in *pgx3-1* mutants (Figures 3F to 3J) and the size and dimensions of mature guard cells in true leaves were normal in adult *pgx3-1* plants (Figures 4C to 4E; Supplemental Table 2), it appears that PGX3 is unlikely to be solely responsible for stomatal pore formation or guard cell expansion. PGX3 may act in concert with other PGs and/or pectate lyases to degrade the middle

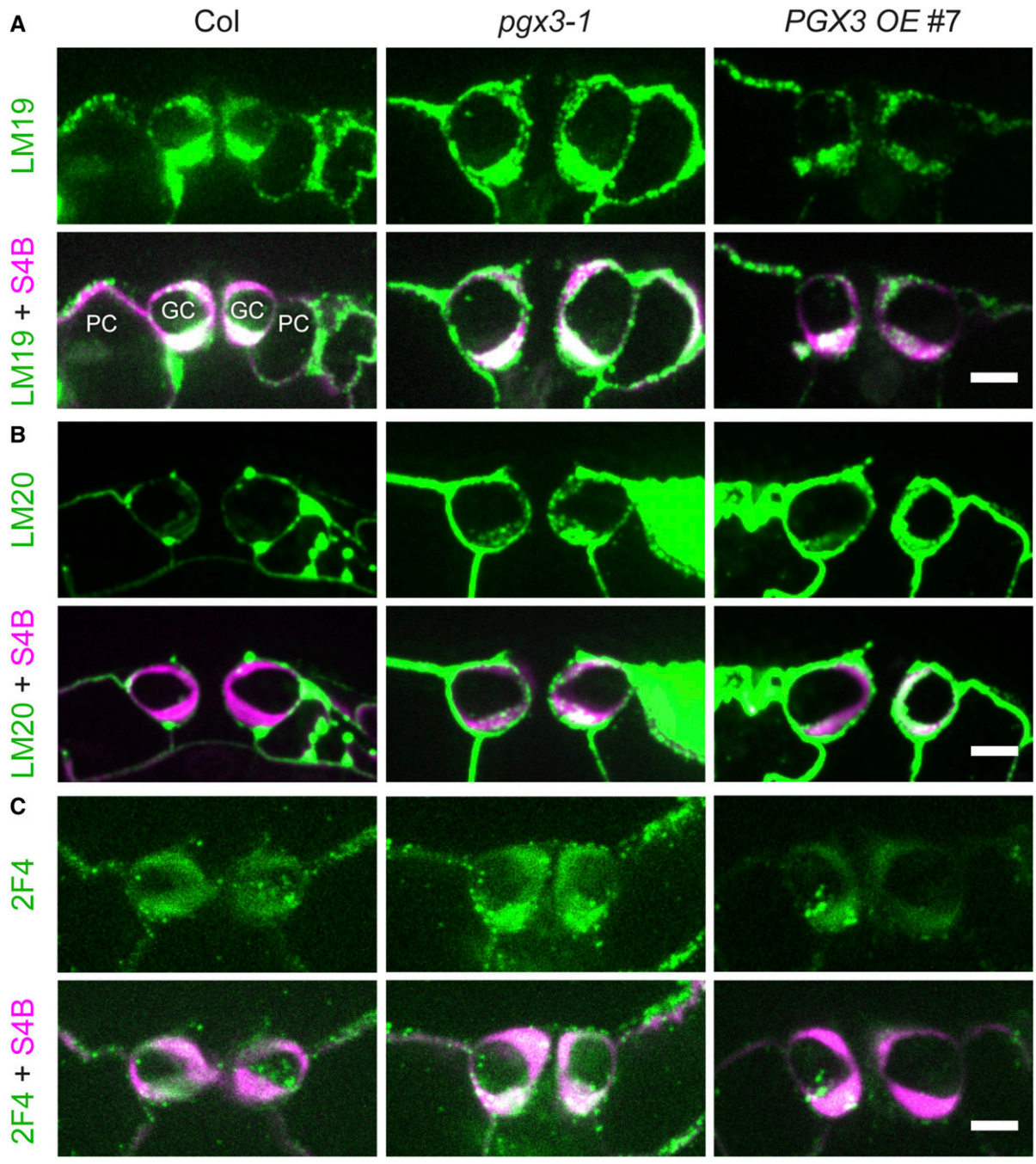

Figure 7. Immunolabeling in Guard Cell Walls Reveals Changes in Antibody Binding.

(A) Colabeling of LM19, an antibody that recognizes demethylesterified HG, and S4B, a dye that binds to cellulose, in cross sections of guard cell pairs in 3- to 4-week-old Col, *pgx3-1*, and *PGX3 OE* #7 plants. Top panels, LM19 labeling; bottom panels, LM19 labeling (green) merged with S4B signals (magenta) in the same guard cell pair. GC, guard cells; PC, pavement cells.
(B) Colabeling of LM20, an antibody that recognizes methylesterified HG, and S4B in cross sections of guard cell pairs in 3- to 4-week-old Col, *pgx3-1*, and *PGX3 OE* #7 plants. Top panels, LM20 labeling; bottom panels, LM20 labeling (green) merged with S4B signals (magenta) in the same guard cell pair.
(C) Colabeling of 2F4, an antibody that recognizes Ca^{2+}-cross-linked HG, and S4B in cross sections of guard cell pairs in 3- to 4-week-old Col, *pgx3-1*, and *PGX3 OE* #7 plants. Top panels, 2F4 labeling; bottom panels, 2F4 labeling (green) merged with S4B signals (magenta) in the same guard cell pair.
Bars = 5 μm in **(A)** to **(C)**.

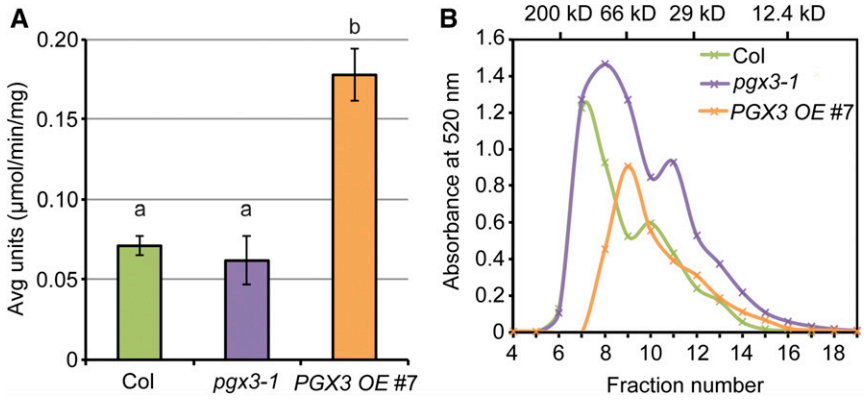

Figure 8. Changes in *PGX3* Expression Level Lead to Altered Total PG Activity and HG Molecular Mass.

(A) Total PG activity in vivo is significantly higher in *PGX3 OE* #7 plants. Total plant proteins were isolated from 33-d-old flowers. One unit of PG activity is the amount of enzyme releasing 1 µmol reducing end group per min per mg total protein at 30°C. Error bars are SE, and lowercase letters represent significantly different groups ($n \geq 3$ technical replicates per genotype per biological replicate, two biological replicates, and each biological replicate is an independent pool of flowers; $P < 0.05$, one-way ANOVA and Tukey test).

(B) Molecular mass analysis of CDTA-soluble pectins extracted from 34-d-old Col, *pgx3-1*, and *PGX3 OE* #7 rosette leaves. Molecular mass of the standards (β-amylase, 200 kD; BSA, 66 kD; carbonic anhydrase, 29 kD; and cytochrome c, 12.4 kD) is shown on the *x* axis at the top ($n = 2$ technical replicates per genotype per biological replicate, two biological replicates, and each biological replicate is an independent pool of rosette leaves).

lamella specifically in the center of the common walls between sister guard cells, but our data nonetheless indicate that pectin degradation is at least one component of the mechanism underlying the cell separation events that result in stomatal pore formation, at least in cotyledons.

Although PGX3-GFP was found to be enriched at stomatal pore initiation sites in cotyledons (Figure 2C), PGX3-GFP was not detectable in guard cells in true leaves (Supplemental Figure 2B), where the *PGX3* promoter was still active (Figures 1F to 1J). This observation could be due to posttranscriptional regulation of *PGX3* when stomata become mature. Alternatively, PGX3-GFP fluorescence might be diminished by the low apoplastic pH of mature leaf cells (Llopis et al., 1998) and/or might be lost against a background of increased chloroplast autofluorescence. These data also suggest that stomata in cotyledons and stomata in true leaves are functionally distinct. This idea is also supported by the observation that although the pore size of developing stomata present in cotyledons was altered when *PGX3* was absent or overexpressed (Figures 3F to 3J), stomatal size and dimensions in mature leaves remained similar to Col controls in *pgx3-1* and *PGX3 OE* plants (Figures 4C to 4E; Supplemental Tables 1 and 2). These results indicate that there might be compensatory PG activity regulating stomatal size in true leaves and exclude the possibility that changes in stomatal dimensions are the cause for the asymmetrically altered stomatal dynamics in *pgx3-1* mutants and *PGX3 OE* plants (Figure 5; Supplemental Figure 7).

Our dye staining (Figure 6) and immunolabeling (Figure 7) results provide direct evidence that PGX3 can regulate guard cell wall composition. The abundance of demethylesterified HG (as detected by COS^{488}, PI, and LM19 antibody) was increased in *pgx3-1* mutants, but reduced in *PGX3 OE* guard cell walls. Immunolabeling data with LM20, JIM7, and 2F4 revealed additional findings regarding other forms of HG. In both *pgx3-1* mutants and *PGX3 OE* plants, labeling intensity for LM20 and JIM7 was elevated relative to Col controls (Figure 7; Supplemental Figures 10 and 11), indicating that methylesterified HG was more abundant and/or more accessible to the antibodies. This is not the first report that loss-of-function and overexpression lines for a *PG* gene displayed the same changes in wall makeup and accessibility relative to the wild type. For example, arabinan content and RG-I extractability by KOH are higher in the walls of both *pgx1* mutants and *PGX1* overexpression plants (Xiao et al., 2014). For the 2F4 antibody, labeling intensity was increased in *pgx3-1* mutants but was reduced in *PGX3 OE* guard cells compared with Col controls (Figure 7C; Supplemental Figure 10C). These results could also be interpreted as changes in the amount and/or accessibility of Ca^{2+}-cross-linked HG.

Different from a previously published work in which 2F4 and LM20 epitopes were not detected in guard cell walls of wild-type Arabidopsis (Amsbury et al., 2016), we observed signals for both antibodies in guard cells and were able to quantify their intensities. This discrepancy could be due to different compositions of buffers used in immunolabeling, especially 2F4 labeling that is usually performed in the presence of Ca^{2+} (Liners et al., 1989; Peaucelle et al., 2008), and/or different durations for primary antibody incubation. The enrichment of binding sites for both small molecule dyes (Figure 6) and all four antibodies (Figure 7; Supplemental Figures 10 and 11) in *pgx3-1* guard cell walls might result from an overall increased amount of extractable HG (Figure 8B), making every form of HG more abundant and/or detectable. Enhanced epitope recognition by LM20 (Figure 7B; Supplemental Figure 10B) and JIM7 (Supplemental Figure 11) in *PGX3 OE* #7 guard cell walls might occur because methylesterified HG is more accessible when demethylesterified HG is excessively degraded and/or because methylesterified HG is more resistant to PG degradation, even when *PGX3* is overexpressed. Alternatively, as a feedback to excessive degradation of demethylesterified HG, more methylesterified HG might be synthesized and delivered to the wall. Consistent with this finding in *PGX3 OE* #7 plants, a recent

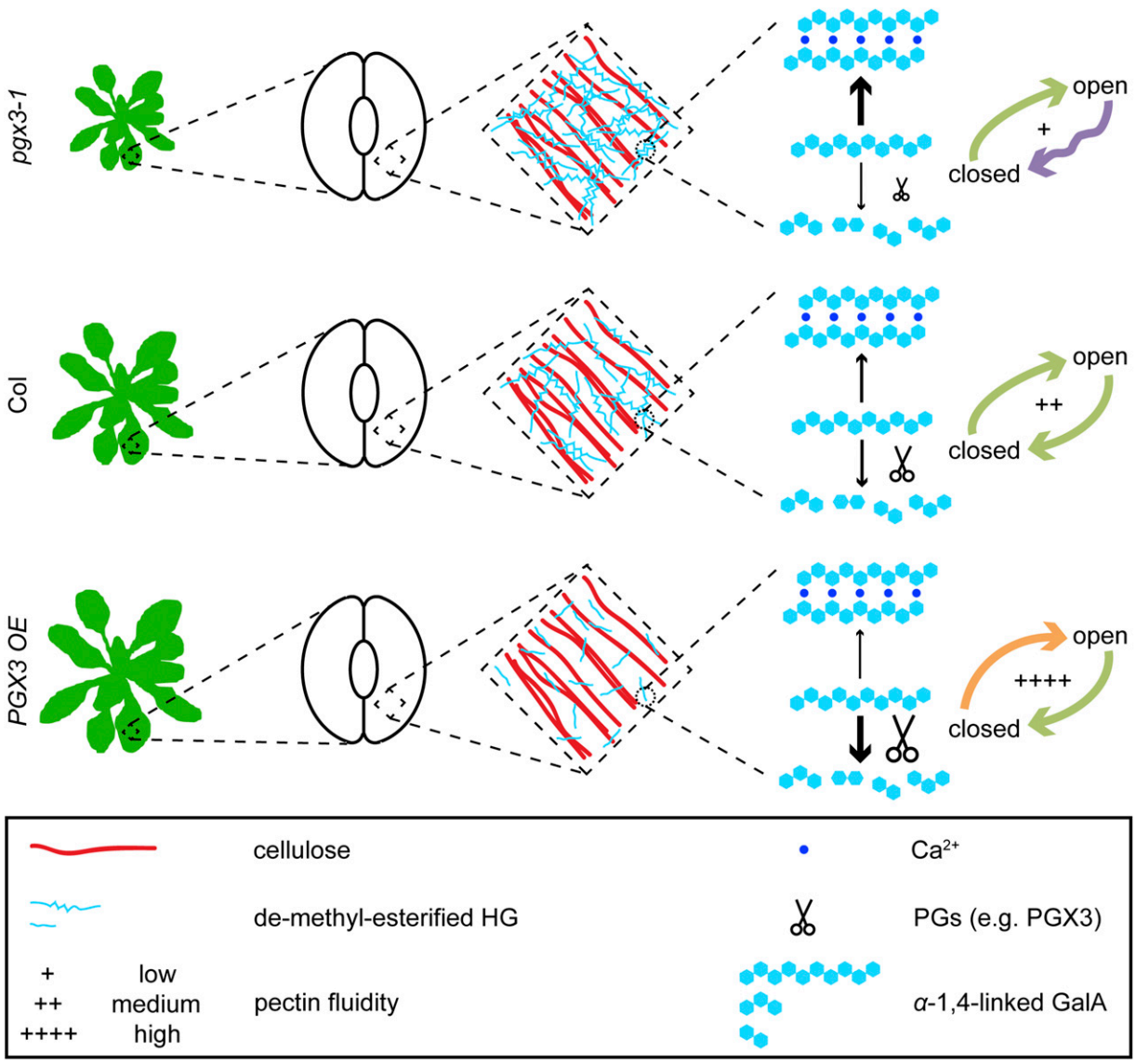

Figure 9. Schematic for How PGX3 Regulates Rosette Expansion and Stomatal Dynamics.

Demethylesterified HG can either be cross-linked by Ca^{2+} or be subject to degradation by PGs such as PGX3. The balance between these two processes maintain pectin fluidity in the walls that undergo irreversible expansion (e.g., in rosettes) and in guard cell walls that undergo reversible expansion and contraction. In *pgx3-1* mutants, although there is no significant change in pectin size due to the absence of *PGX3* expression, Ca^{2+}-cross-linked HG formation occurs more frequently because the abundance of demethylesterified HG is increased. As a result, pectin fluidity is lessened and tissue growth is inhibited. Stomata exhibit stepwise closure, but guard cell walls are still fluid enough to allow for normal stomatal opening. In Col controls, pectin fluidity is maintained at intermediate levels due to a balance between Ca^{2+}-cross-linking and pectin degradation, enabling normal stomatal opening or closure. In *PGX3 OE* plants, HG molecules are smaller due to excessive *PGX3* expression and more pectin degradation, which, together with the observation that there is less demethylesterified HG, leads to enhanced pectin fluidity, increased rosette size, and faster stomatal opening.

solid-state NMR study reveals a higher degree of HG methyl-esterification in $PGX1^{AT}$ cell walls (Phyo et al., 2017), which, along with smaller average pectin molecular weight, correlates with enhanced growth in $PGX1^{AT}$ plants (Xiao et al., 2014).

The interrelationship of the biochemical and biophysical properties of plant cell walls has been intensively studied, but not fully elucidated. In Arabidopsis, alterations in cell wall biochemistry have been examined for their effects on tissue mechanics and morphogenesis (Peaucelle et al., 2011, 2015), but much less so for their effects on individual cellular behaviors, especially stomatal dynamics. Recently, stomatal guard cell walls of Arabidopsis were reported to be enriched in demethylesterified pectins, and mutants lacking *PME6* display both enhanced pectin methylesterification and narrower ranges of stomatal responses to stimuli (Amsbury et al., 2016). These data imply that aberrant stomatal behaviors might be caused by altered wall mechanics in *pme6* guard cells

(Amsbury et al., 2016), but it is currently mysterious how PME6 regulates these mechanics because removing methyl groups from pectins might result in either wall stiffening or loosening, depending on the patterns of demethylesterification (Levesque-Tremblay et al., 2015; Hocq et al., 2017). Additionally, *PME34* has been implicated in stomatal responses to heat stress in Arabidopsis (Huang et al., 2017), suggesting that multiple pectin methylesterases might modulate pectin cross-linking and/or degradability in guard cell walls, adding an additional layer of complexity and control. Pectin-degrading enzymes, including PGs and PLs, act downstream of PMEs during pectin modification and autodegradation, and it remains to be tested which PGs and/or PLs are affected in *pme* mutants, either in expression or specific activity.

From a mechanical perspective, we propose the following scenarios for the asymmetric alterations in stomatal dynamics that we observed when *PGX3* is absent or overexpressed. Guard cell walls are compressed during stomatal closure (DeMichele and Sharpe, 1973). The resulting compressive stress may push fluidic wall components, such as pectins, through the incompressible cellulose network. In *pgx3-1* guard cell walls, increased levels of demethylesterified HG (Figures 6, 7A, and 8B; Supplemental Figure 10A) may result in higher viscosity (lower fluidity) in pectic matrices. Assuming the spacing in cellulose networks is consistent (Supplemental Figures 8A and 8B), more HG molecules will be enmeshed within the cellulose network, resulting in momentarily and locally elevated stiffness in the guard cell wall. When the increased stress exceeds a certain threshold, the guard cell wall will spontaneously compress, resulting in a stepwise decrease in stomatal pore width (Figure 5B; Supplemental Figure 7A). In addition, intermolecularly cross-linked networks of HG are possibly stronger in *pgx3-1* guard cell walls (Figure 7C; Supplemental Figure 10C), further preventing smooth stomatal closure. In contrast, guard cell walls undergo tensile deformation during stomatal opening. Reduced levels of demethylesterified HG (Figures 6, 7A, and 8B; Supplemental Figure 10A), smaller pectin size (Figure 8B), and possibly less Ca^{2+} cross-linking (Figure 7C; Supplemental Figure 10C) result in lower stiffness (higher compliance) of guard cell walls in *PGX3 OE* plants, making them less resistant against extension and allowing for more rapid stomatal opening (Figure 5A; Supplemental Figure 7B). Interestingly, during stomatal opening or closure, the initial and the final stomatal pore widths remained largely unaltered by changes in *PGX3* expression levels (Figures 5A and 5B; Supplemental Figures 7A and 7B and Supplemental Tables 1 and 2), suggesting that PGX3 possesses functions that are distinct from PME6 (Amsbury et al., 2016), which sets the overall range of pore width during stomatal movement. Instead, PGX3 regulates stomatal dynamics by maintaining guard cell wall elasticity during both compressive and tensile deformations.

Finally, using experimental data and nonlinear mathematical fits of stomatal opening and closure (Supplemental Figure 12), we generated a conceptual model (Figure 9) summarizing the proposed effects of PGX3 activity on pectin network remodeling during rosette expansion and during stomatal movements as driven by changes in turgor pressure (Kollist et al., 2014). We propose that, in the cell walls of Col plants, a balance between HG cross-linking and degradation during development results in the formation of HG networks that can undergo continuous, cyclic HG uncoupling/Ca^{2+} release and cross-linking. This allows for normal tissue growth, smooth stomatal opening in pressurizing guard cells, and smooth closure in depressurizing guard cells. In *pgx3-1* mutants, excessive HG abundance and/or cross-linking inhibits tissue expansion and smooth stomatal closure, but still allows for Ca^{2+} release during stomatal opening. By contrast, in *PGX3 OE* cells, lower demethylesterified HG levels and smaller HG size results in enhanced tissue size and accelerated stomatal opening in response to pressurization, although these levels might still be sufficient for the smooth remodeling of HG networks during stomatal closure. Further analyses of stomatal dynamics in other mutants with altered pectin networks and in other species will help to refine and generalize this model.

In summary, the data presented here provide new insights into how guard cell walls are constructed to confer their specific biomechanical properties and meet their functional requirements: Along with cellulose and xyloglucan, which help control the anisotropic expansion of guard cells (Rui and Anderson, 2016; Woolfenden et al., 2017), and structural glycoproteins, which also influence guard cell flexibility (Hunt et al., 2017), characterization of PGX3 highlights its key function as a pectinase in guard cell walls that regulates the dynamics of guard cells, allowing them to maintain high integrity and flexibility during stomatal movements in Arabidopsis. Further understanding of the synthesis, composition, architecture, modifications, and dynamics of guard cell walls will have promising applications across many fields, including the design of biomaterials with useful mechanical properties and the production of plants with desirable stomatal traits.

METHODS

Plant Materials and Growth Conditions

Arabidopsis thaliana seeds (Col-0 background) were surface sterilized in 30% bleach containing 0.1% SDS, washed four times with sterile water, and sown on Murashige and Skoog plates (0.6 g/L MES, 1% or 0% [w/v] sucrose, and 0.8% agar, pH 5.6). Seedlings were grown vertically at 22°C under 24-h illumination. Ten-day-old seedlings were transferred from plates into Fafard C2 soil (Griffin Greenhouse) supplemented with Miracle-Gro (The Scotts Company; catalog no. 1001233), and plants were grown in a chamber at 22°C with a 16-h-light/8-h-dark photoperiod.

Transgenic Lines

A 2072-bp promoter-containing fragment upstream of the *PGX3* start codon was amplified from Col genomic DNA and cloned into pMDC162 (Curtis and Grossniklaus, 2003), which contains the *GUS* coding sequence, to generate a *ProPGX3:GUS* construct, which was then transformed into Col plants using the floral dip method (Clough and Bent, 1998). Transgenic lines were selected on Murashige and Skoog plates with 25 μg/mL hygromycin. For subcellular localization analyses, the same 2072-bp fragment and the full *PGX3* CDS were amplified from Col genomic DNA and Col cDNA, respectively, using Phusion hot start high-fidelity DNA Polymerase (Thermo Fisher) and gene-specific primers (Supplemental Table 3). They were then ligated by overlap PCR (Lu, 2005) and the final product was cloned into pMDC110 (Curtis and Grossniklaus, 2003) to generate the *ProPGX3:PGX3-GFP* construct, which was then transformed into Col and *pgx3-1* mutant plants, respectively. Transgenic lines were selected with 25 μg/mL hygromycin. *pgx3-1* mutants expressing *ProPGX3:PGX3-GFP* were generated and designated as *PGX3 comp*. For constitutive overexpression, the *PGX3* coding sequence was cloned into pEarleyGate101

(Earley et al., 2006) to generate a *Pro35S:PGX3-YFP* construct, which was then transformed into Col plants to generate *PGX3 OE* lines, which were selected using 5 μM methionine sulfoximine.

Gene Expression Analyses

Tissues of transgenic plants expressing *ProPGX3:GUS* were stained in 50 mM sodium phosphate, pH 7.2, 0.2% (v/v) Triton X-100, and 2 mM 5-bromo-4-chloro-3-indoxyl-β-D-glucuronide cyclohexylammonium salt (X-Gluc) in the dark at 37°C for 3 to 16 h. Tissues were destained with 70% ethanol, and images were collected on a Zeiss Discovery V12 fluorescence dissecting microscope. For qPCR, total RNA was extracted from different tissues of Col plants using a plant RNA isolation kit (Omega Bio-Tek), and genomic DNA was removed by RNase-free DNase I (NEB). cDNA was synthesized using Quanta qScript cDNA Supermix (Quantabio). qPCR was performed using Quanta PerfeCTa SYBR Green Fastmix ROX (Quantabio; catalog no. 95073-250) with gene-specific primers (Supplemental Table 3) on a StepOne Plus Real-Time PCR machine (Applied Biosystems). Double-stranded DNA products were detected by the SYBR Green dye in the Fastmix, and *PGX3* transcript levels relative to *ACTIN2* (*ACT2*) were calculated using the ΔΔCt method. *PGX3* expression in 6-d-old etiolated hypocotyls was normalized to 1. Three biological replicates were used for each tissue and each biological replicate was an independent pool of tissues. For example, for 6-d-old etiolated hypocotyls, each biological replicate contained ~40 dark-grown seedlings. For 3-week-old rosette leaves, each biological replicate contained two to three rosette leaves collected from two to three individual plants.

Plant Growth Analysis and Segmentation of Rosette Images

Seedlings on plates were scanned on a Scanjet 8300 scanner (HP) at 600 dpi. Root length and hypocotyl length were measured in ImageJ (W.S. Rasband, U. S. National Institutes of Health, Bethesda, MD; https://imagej.nih.gov/ij/). Relative growth rate of roots was calculated on an individual basis. Rosette images were taken with a Nikon D5100 DSLR camera and were computationally segmented. Raw rosette images were in the RGB color space, and were converted to the HSV (hue, saturation, and value) color space using the OpenCV image processing software library (Bradski, 2000). A single range of green colors was chosen from the histogram of hue values to separate the foreground rosette from the background. Threshold cutoffs were applied to obtain green areas with elevated saturation values according to this range. The binary image masks were morphologically processed to fill holes and remove small artifacts in the background. The foreground regions delineated by the mask were selected from the original image. Segmented images were analyzed in ImageJ for rosette area using the wand tool. In growth assays, Col control seedlings or plants were always grown side by side with any of the mutants or transgenic lines tested.

Stomatal Function Assays

In each stomatal function assay, Col controls grown side by side under identical conditions were used to avoid any deviations in stomatal pore width caused by environmental fluctuations. Stomatal opening and closure assays were performed as described (Rui and Anderson, 2016). In brief, stomatal opening was induced by applying 1 μM FC or light treatment to excised leaves, whereas stomatal closure was induced by applying 50 μM ABA or dark treatment to excised leaves, after which epidermal peels of treated leaves were imaged by transmission light microscopy for geometric measurements of stomata.

Stomatal Dynamics Analysis

To analyze ABA-induced stomatal closure dynamics, rosette leaves of 3- to 4-week-old Col, *pgx3-1*, and *PGX3 OE* #7 plants were incubated in a solution containing 20 mM KCl, 1 mM $CaCl_2$, and 5 mM MES-KOH, pH 6.15, in the light for 2.5 h to cause stomatal opening. Epidermal peels were made from the abaxial side of leaves. In each independent experiment, one Col epidermal peel and one *pgx3-1* epidermal peel, or one Col epidermal peel and one *PGX3 OE* #7 epidermal peel were placed side-by-side on the same slide. ABA (50 μM) in the same solution as above was added onto the slide to induce stomatal closure. Slides were sealed with vacuum grease to avoid evaporation. Bright-field images were taken on the confocal with a 63× objective immediately after adding ABA and every 10 min thereafter at the same positions for each genotype. Images were collected at room temperature in the light (with the transmission light and room light on throughout the experiment). For light-induced stomatal opening dynamics, rosette leaves of 3- to 4-week-old Col and *PGX3 OE* #7 plants were incubated in a solution containing 50 mM KCl, 0.1 mM $CaCl_2$, and 10 mM MES-KOH, pH 6.15, in the dark for 2.5 h to cause stomatal closure. Epidermal peels were made from the abaxial side of leaves. In each independent experiment, one Col epidermal peel and one *PGX3 OE* #7 epidermal peel were placed side by side on the same slide. The incubation solution was added onto the slide. Slides were sealed with vacuum grease to avoid evaporation. Bright-field images were taken immediately and 10 min thereafter at the same position for each genotype. Stomatal opening was induced by light with both room light and transmission light on throughout the experiment. Kymographs were generated in ImageJ by drawing a line across the width of the stomatal pore to show the trajectories of changes in stomatal pore width.

Confocal Microscopy

Confocal images were collected on a Zeiss Axio Observer microscope with a Yokogawa CSU-X1 spinning disk head and a 63× or a 100× 1.4 NA oil immersion objective. A 488-nm excitation laser and a 525/550-nm emission filter were used for detection of GFP and COS^{488}, which binds to negatively charged carboxyl groups on stretches of demethylesterified GalA residues in HG (Mravec et al., 2014). A 561-nm excitation laser and a 617/673-nm emission filter were used to image PI. Subcellular localization analyses in roots were performed in either 5-d-old seedlings expressing *ProPGX3:PGX3-GFP* or Col control seedlings. Some seedlings were plasmolyzed with 1 M mannitol for 5 min to test whether PGX3-GFP associates with the wall or the plasma membrane. Subcellular localization in developing stomata was observed in 4-d-old seedlings stained with 100 μg/mL PI (Life Technologies) for 5 min. For COS^{488} labeling, 3- to 4-week-old rosette leaves were stained with COS^{488} diluted at 1:1000 in 25 mM MES, pH 5.7, for 20 min, washed with MES buffer, and mounted in MES buffer and glycerol at 1:1. For PI staining, 6-d-old seedlings or 3- to 4-week-old rosette leaves were stained as described above. Fluorescence intensities of COS^{488} or PI were quantified as described previously (Rui and Anderson, 2016) with a region of interest defined as in Supplemental Figure 8C. S4B staining in guard cells was performed as described previously (Rui and Anderson, 2016). For measurements of stomatal density, stomatal index, stomatal complex size, and pavement cell size, 1-, 2-, 3-, and 4-week-old true leaves of Col, *pgx3-1*, *PGX3 comp* #3, and *PGX3 OE* #7 were stained with 100 μg/mL PI, and snapshot images were taken on the confocal microscope with a 20× or a 63× objective. Quantifications were then performed using ImageJ.

Immunolabeling

Immunolabeling of guard cells was performed as described by Amsbury et al. (2016), with the following modifications. Three- to four-week-old Arabidopsis rosette leaves of Col, *pgx3-1*, *PGX3 OE* #7 plants were first trimmed into 3 × 3-mm squares and fixed in 4% paraformaldehyde in PEM buffer (0.1 M PIPES, 2 mM EGTA, and 1 mM $MgSO_4$, pH 7.0) with vacuum infiltration for 0.5 to 1 h. Leaf cuts were then rinsed in PEM buffer,

dehydrated in an ethanol series (30, 50, 70, and 100% ethanol), and infiltrated with a series of LR White resin (a polyhydroxylated aromatic acrylic resin) (Electron Microscopy Sciences; 10, 20, 30, 50, 70, 90, and 100%) diluted in ethanol. Samples were embedded vertically in gelatin capsules (Ted Pella) and resin polymerization was performed at 37°C for 7 d. Thin sections (2 μm thick) were cut on a Leica UC6 ultramicrotome with a glass knife. For immunolabeling with LM19 (PlantProbes, University of Leeds; catalog no. LM19), LM20 (PlantProbes; catalog no. LM20), and JIM7 (CCRC, University of Georgia; catalog no. JIM7), sections were first blocked in KPBS buffer (0.01 M K_3PO_4 and 0.5 M NaCl, pH 7.1) with 3% BSA for at least 3 h. Sections were then incubated with a primary antibody at 1:10 dilution in KPBS buffer with 3% BSA in a humidified chamber at room temperature for 24 h. Samples were rinsed with KPBS buffer three times and incubated with Alexa Fluor 488-conjugated goat anti-rat IgG (H+L) (Jackson ImmunoResearch Laboratories; catalog no. 112-546-003) at 1:100 dilution in KPBS buffer with 3% BSA in the dark for 16 h. Sections were rinsed again with KPBS buffer three times before staining with 0.1% (w/v) S4B in KPBS buffer in the dark for 30 min. For 2F4 (PlantProbes; catalog no. 2F4) immunolabeling (1:10 dilution), Alexa Fluor 488-conjugated goat anti-mouse IgG (H+L) (Jackson ImmunoResearch Laboratories; catalog no. 115-546-003) was used at 1:100 dilution, and TCaS buffer (20 mM Tris-HCl, 0.5 mM $CaCl_2$, and 150 mM NaCl, pH 8.2) was used instead of KPBS buffer throughout the procedure because 2F4 immunolabeling does not work in conventional PBS buffer (Liners et al., 1989; Peaucelle et al., 2008). Images of immunolabeled sections were collected on a Zeiss Axio Observer microscope with a Yokogawa CSU-X1 spinning disk head and a 100× 1.4 NA oil immersion objective, with a 488-nm excitation laser and a 525/550-nm emission filter for Alexa Fluor 488 signals and a 561-nm excitation laser and a 617/673-nm emission filter for S4B signals. For a given primary antibody, the same settings of laser power, exposure time, and CCD gain values were always applied to both primary antibody-incubated sections and control sections across genotypes. Immunolabeling fluorescence intensities were analyzed as described (Peaucelle et al., 2015). In brief, guard cell wall area was determined by S4B staining signals. The same area was applied to the corresponding immunolabeling image as a region of interest and raw integrated density was recorded. The fluorescence intensity of each antibody was presented as a ratio of raw integrated density to area. The fluorescence intensity in guard cell walls without primary antibody incubated was used as a negative control to subtract background fluorescence.

Total Protein Extraction and Polygalacturonase Activity Assays

Flowers of 33-d-old Col, *pgx3-1*, and *PGX3 OE* #7 plants were ground in liquid N_2, and ~4 mL of fine powder was used for each genotype. Total protein extraction and PG activity assays were performed as described (Xiao et al., 2017, 2014). In brief, total plant proteins were extracted in a buffer containing 50 mM Tris-HCl (pH 7.5), 1 M NaCl, 3 mM EDTA, 2.5 mM 1,4-dithiothreitol (Sigma-Aldrich), 2 mM phenylmethylsulfonyl fluoride (Sigma-Aldrich), and 10% (v/v) glycerol, and were then dialyzed in 50 mM sodium acetate buffer (pH 5.0). Polygalacturonase activity was assessed by measuring the increase in reducing end groups (Gross, 1982), using 0.2% (w/v) polygalacturonic acid (Sigma-Aldrich) as a substrate and D-galacturonic acid (Sigma-Aldrich) as a standard.

Size-Exclusion Chromatography and Uronic Acid Assays

Rosette leaves of 34-d-old Col, *pgx3-1*, and *PGX3 OE* #7 plants grown under long-day conditions were harvested after dark treatment for 24 h and ground into fine powder in liquid nitrogen. The powder was washed with 70% ethanol after treatment with chloroform/methanol (1:1, v/v). The air-dried wall residue was used for pectin extraction as described (Xiao et al., 2017, 2014). Size-exclusion chromatography and uronic acid assays were performed as described (Xiao et al., 2017, 2014). Samples of 150 μL dissolved in 0.1 M sodium acetate buffer were directly loaded into the FPLC loop through the valve. Thirty fractions of 250 μL each were collected and analyzed for uronic acid content.

Statistics

All statistical analyses in this study were performed using the PAST software package (Hammer et al., 2001).

Accession Numbers

Sequence data from this article can be found in the Arabidopsis Genome Initiative or GenBank/EMBL databases under the following accession numbers: *PGX3* (At1g48100), *LTI6b* (At3g05890), and *ACT2* (At3g18780). Mutant germplasm used included *pgx3-1* (SALK_010192C), *pgx3-2* (SALK_019868), and *pgx3-3* (SALK_022923C).

Supplemental Data

Supplemental Figure 1. Phylogenetic Analysis of the Polygalacturonase Family and the Schematic Protein Domains of PGX3.

Supplemental Figure 2. Negative Controls for PI-Stained Stomata in 4-d-Old Col Seedlings and No Detectable PGX3-GFP Signals in 3-Week-Old Rosette Leaves.

Supplemental Figure 3. *PGX3* Gene Structure and Transcript Detection.

Supplemental Figure 4. *PGX3* Functions in Seed Germination, Etiolated Hypocotyl Elongation, and Root Elongation.

Supplemental Figure 5. Hypocotyl Growth and Root Length Are Enhanced in an Additional *PGX3* Overexpression Line.

Supplemental Figure 6. Rosette Phenotypes in Other *PGX3* Complementation and Overexpression Lines.

Supplemental Figure 7. *PGX3* Regulates Dark- or Light-Induced Stomatal Dynamics in True Leaves.

Supplemental Figure 8. Cellulose Organization in *pgx3-1* Mutant Guard Cells and Pectin Labeling by COS^{488} or PI in Guard Cells and Neighboring Pavement Cells.

Supplemental Figure 9. Controls for Immunolabeling in Guard Cell Walls.

Supplemental Figure 10. Quantifications of LM19, LM20, and 2F4 Immunolabeling Intensity in Guard Cell Walls.

Supplemental Figure 11. JIM7 Immunolabeling in Guard Cell Walls.

Supplemental Figure 12. Mathematical Fits of Stomatal Opening and Closure in Col, *pgx3-1*, and *PGX3 OE* #7 Plants.

Supplemental Table 1. Measurement of Stomatal Pore Dimensions, Guard Cell Pair Dimensions, and Guard Cell Dimensions in Wild Type and *PGX3 OE* #7 Plants during FC Treatment.

Supplemental Table 2. Measurement of Stomatal Pore Dimensions, Guard Cell Pair Dimensions, and Guard Cell Dimensions in Wild Type and *pgx3-1* Mutants during ABA Treatment.

Supplemental Table 3. Primers Used in This Study.

Supplemental Movie 1. Stomatal Closure Dynamics in Col Controls, *pgx3-1* Mutants, and *PGX3 OE* #7 Plants in Response to 50 μM ABA.

Supplemental Movie 2. Stomatal Opening Dynamics in Col Controls and *PGX3 OE* #7 Plants in Response to Light.

Supplemental File 1. ANOVA Tables.

ACKNOWLEDGMENTS

We thank Liza Wilson for assistance with pectin molecular weight determination, Juan Du for assistance with protein extraction, Jozef Mravec for providing the COS[488] probe, and members of the Anderson lab, especially Will Barnes, for helpful advice and discussions. Research supplies were purchased with support from a Huck Dissertation Research Award to Y.R. Pectin molecular mass and PG activity were measured with support from the Center for Lignocellulose Structure and Formation, an Energy Frontier Research Center funded by the U.S. Department of Energy, Office of Science, Basic Energy Sciences (Award DE-SC0001090). All other research and manuscript preparation were supported by National Science Foundation Grant MCB-1616316 to C.T.A., V.M.P., and J.Z.W.

AUTHOR CONTRIBUTIONS

Y.R., C.X., and C.T.A. designed experiments. Y.R. and C.X. performed experiments. Y.R., C.X., B.K., H.Y., J.Z.W., V.M.P., and C.T.A. analyzed results. Y.R., C.X., H.Y., B.K., J.Z.W., V.M.P., and C.T.A. wrote the manuscript.

Received July 18, 2017; revised September 5, 2017; accepted October 2, 2017; published October 3, 2017.

REFERENCES

Amsbury, S., Hunt, L., Elhaddad, N., Baillie, A., Lundgren, M., Verhertbruggen, Y., Scheller, H.V., Knox, J.P., Fleming, A.J., and Gray, J.E. (2016). Stomatal function requires pectin de-methylesterification of the guard cell wall. Curr. Biol. **26:** 2899–2906.

Anderson, C.T., Carroll, A., Akhmetova, L., and Somerville, C. (2010). Real-time imaging of cellulose reorientation during cell wall expansion in Arabidopsis roots. Plant Physiol. **152:** 787–796.

Atkinson, R.G., Schröder, R., Hallett, I.C., Cohen, D., and MacRae, E.A. (2002). Overexpression of polygalacturonase in transgenic apple trees leads to a range of novel phenotypes involving changes in cell adhesion. Plant Physiol. **129:** 122–133.

Atmodjo, M.A., Hao, Z., and Mohnen, D. (2013). Evolving views of pectin biosynthesis. Annu. Rev. Plant Biol. **64:** 747–779.

Bates, G.W., Rosenthal, D.M., Sun, J., Chattopadhyay, M., Peffer, E., Yang, J., Ort, D.R., and Jones, A.M. (2012). A comparative study of the *Arabidopsis thaliana* guard-cell transcriptome and its modulation by sucrose. PLoS One **7:** e49641.

Bergmann, D.C., and Sack, F.D. (2007). Stomatal development. Annu. Rev. Plant Biol. **58:** 163–181.

Boyer, J.S. (2016). Enzyme-less growth in Chara and terrestrial plants. Front. Plant Sci. **7:** 866.

Bradski, G. (2000). The opencv library. Dr. Dobbs J. Softw. Tools Prof. Program. **5:** 6.

Braybrook, S.A., and Jönsson, H. (2016). Shifting foundations: the mechanical cell wall and development. Curr. Opin. Plant Biol. **29:** 115–120.

Clough, S.J., and Bent, A.F. (1998). Floral dip: a simplified method for Agrobacterium-mediated transformation of *Arabidopsis thaliana*. Plant J. **16:** 735–743.

Cosgrove, D.J. (2014). Re-constructing our models of cellulose and primary cell wall assembly. Curr. Opin. Plant Biol. **22:** 122–131.

Curtis, M.D., and Grossniklaus, U. (2003). A gateway cloning vector set for high-throughput functional analysis of genes in planta. Plant Physiol. **133:** 462–469.

Cutler, S.R., Ehrhardt, D.W., Griffitts, J.S., and Somerville, C.R. (2000). Random GFP:cDNA fusions enable visualization of subcellular structures in cells of Arabidopsis at a high frequency. Proc. Natl. Acad. Sci. USA **97:** 3718–3723.

DeMichele, D.W., and Sharpe, P.J.H. (1973). An analysis of the mechanics of guard cell motion. J. Theor. Biol. **41:** 77–96.

Earley, K.W., Haag, J.R., Pontes, O., Opper, K., Juehne, T., Song, K., and Pikaard, C.S. (2006). Gateway-compatible vectors for plant functional genomics and proteomics. Plant J. **45:** 616–629.

González-Carranza, Z.H., Elliott, K.A., and Roberts, J.A. (2007). Expression of polygalacturonases and evidence to support their role during cell separation processes in *Arabidopsis thaliana*. J. Exp. Bot. **58:** 3719–3730.

Gross, K.C. (1982). A rapid and sensitive spectrophotometric method for assaying polygalacturonase using 2-cyanoacetamide. HortScience **17:** 933–934.

Hachez, C., Ohashi-Ito, K., Dong, J., and Bergmann, D.C. (2011). Differentiation of Arabidopsis guard cells: analysis of the networks incorporating the basic helix-loop-helix transcription factor, FAMA. Plant Physiol. **155:** 1458–1472.

Hammer, Ø., Harper, D.A.T., and Ryan, P.D. (2001). PAST: paleontological statistics software package for education and data analysis. Palaeontol. Electronica **4:** 1–9.

Hocq, L., Pelloux, J., and Lefebvre, V. (2017). Connecting homogalacturonan-type pectin remodeling to acid growth. Trends Plant Sci. **22:** 20–29.

Huang, Y.C., Wu, H.C., Wang, Y.D., Liu, C.H., Lin, C.C., Luo, D.L., and Jinn, T.L. (2017). PECTIN METHYLESTERASE34 contributes to heat tolerance through its role in promoting stomatal movement. Plant Physiol. **174:** 748–763.

Hunt, L., Amsbury, S., Baillie, A., Movahedi, M., Mitchell, A., Afsharinafar, M., Swarup, K., Denyer, T., Hobbs, J.K., Swarup, R., Fleming, A.J., and Gray, J.E. (2017). Formation of the stomatal outer cuticular ledge requires a guard cell wall proline-rich protein. Plant Physiol. **174:** 689–699.

Jones, L., Milne, J.L., Ashford, D., McCann, M.C., and McQueen-Mason, S.J. (2005). A conserved functional role of pectic polymers in stomatal guard cells from a range of plant species. Planta **221:** 255–264.

Jones, L., Milne, J.L., Ashford, D., and McQueen-Mason, S.J. (2003). Cell wall arabinan is essential for guard cell function. Proc. Natl. Acad. Sci. USA **100:** 11783–11788.

Kim, J., Shiu, S.H., Thoma, S., Li, W.H., and Patterson, S.E. (2006). Patterns of expansion and expression divergence in the plant polygalacturonase gene family. Genome Biol. **7:** R87.

Knox, J.P., Linstead, P.J., King, J., Cooper, C., and Roberts, K. (1990). Pectin esterification is spatially regulated both within cell walls and between developing tissues of root apices. Planta **181:** 512–521.

Kollist, H., Nuhkat, M., and Roelfsema, M.R. (2014). Closing gaps: linking elements that control stomatal movement. New Phytol. **203:** 44–62.

Levesque-Tremblay, G., Pelloux, J., Braybrook, S.A., and Müller, K. (2015). Tuning of pectin methylesterification: consequences for cell wall biomechanics and development. Planta **242:** 791–811.

Liners, F., Letesson, J., Didembourg, C., and Cutsem, P.V. (1989). Monoclonal antibodies against pectins: recognition of a conformation induced by calcium. Plant Physiol. **91:** 1419–1424.

Llopis, J., McCaffery, J.M., Miyawaki, A., Garquhar, M.G., and Tsien, R. (1998). Measurement of cytosolic, mitocondrial, and Golgi pH in single living cells with green fluorescent proteins. Proc. Natl. Acad. Sci. USA **95:** 6803–6808.

Lu, Q. (2005). Seamless cloning and gene fusion. Trends Biotechnol. **23:** 199–207.

Majewska-Sawka, A., Münster, A., and Rodríguez-García, M.I. (2002). Guard cell wall: immunocytochemical detection of polysaccharide components. J. Exp. Bot. **53:** 1067–1079.

McCarthy, T.W., Der, J.P., Honaas, L.A., dePamphilis, C.W., and Anderson, C.T. (2014). Phylogenetic analysis of pectin-related gene families in *Physcomitrella patens* and nine other plant species yields evolutionary insights into cell walls. BMC Plant Biol. **14:** 79.

Mravec, J., et al. (2014). Tracking developmentally regulated post-synthetic processing of homogalacturonan and chitin using reciprocal oligosaccharide probes. Development **141:** 4841–4850.

Ogawa, M., Kay, P., Wilson, S., and Swain, S.M. (2009). ARABIDOPSIS DEHISCENCE ZONE POLYGALACTURONASE1 (ADPG1), ADPG2, and QUARTET2 are polygalacturonases required for cell separation during reproductive development in Arabidopsis. Plant Cell **21:** 216–233.

Ohashi-Ito, K., and Bergmann, D.C. (2006). Arabidopsis FAMA controls the final proliferation/differentiation switch during stomatal development. Plant Cell **18:** 2493–2505.

Pandey, S., Wang, R.S., Wilson, L., Li, S., Zhao, Z., Gookin, T.E., Assmann, S.M., and Albert, R. (2010). Boolean modeling of transcriptome data reveals novel modes of heterotrimeric G-protein action. Mol. Syst. Biol. **6:** 372.

Peaucelle, A., Louvet, R., Johansen, J.N., Höfte, H., Laufs, P., Pelloux, J., and Mouille, G. (2008). Arabidopsis phyllotaxis is controlled by the methyl-esterification status of cell-wall pectins. Curr. Biol. **18:** 1943–1948.

Peaucelle, A., Braybrook, S.A., Le Guillou, L., Bron, E., Kuhlemeier, C., and Höfte, H. (2011). Pectin-induced changes in cell wall mechanics underlie organ initiation in Arabidopsis. Curr. Biol. **21:** 1720–1726.

Peaucelle, A., Wightman, R., and Höfte, H. (2015). The control of growth symmetry breaking in the Arabidopsis hypocotyl. Curr. Biol. **25:** 1746–1752.

Phyo, P., Wang, T., Xiao, C., Anderson, C.T., and Hong, M. (2017). Effects of pectin molecular weight changes on the structure, dynamics, and polysaccharide interactions of primary cell walls of *Arabidopsis thaliana*: Insights from solid-state NMR. Biomacromolecules **18:** 2937–2950.

Pillitteri, L.J., and Torii, K.U. (2012). Mechanisms of stomatal development. Annu. Rev. Plant Biol. **63:** 591–614.

Rhee, S.Y., Osborne, E., Poindexter, P.D., and Somerville, C.R. (2003). Microspore separation in the quartet 3 mutants of Arabidopsis is impaired by a defect in a developmentally regulated polygalacturonase required for pollen mother cell wall degradation. Plant Physiol. **133:** 1170–1180.

Rhee, S.Y., and Somerville, C.R. (1998). Tetrad pollen formation in quartet mutants of *Arabidopsis thaliana* is associated with persistence of pectic polysaccharides of the pollen mother cell wall. Plant J. **15:** 79–88.

Rounds, C.M., Lubeck, E., Hepler, P.K., and Winship, L.J. (2011). Propidium iodide competes with Ca^{2+} to label pectin in pollen tubes and Arabidopsis root hairs. Plant Physiol. **157:** 175–187.

Rui, Y., and Anderson, C.T. (2016). Functional analysis of cellulose and xyloglucan in the walls of stomatal guard cells of Arabidopsis. Plant Physiol. **170:** 1398–1419.

Shtein, I., Shelef, Y., Marom, Z., Zelinger, E., Schwartz, A., Popper, Z.A., Bar-On, B., and Harpaz-Saad, S. (2017). Stomatal cell wall composition: distinctive structural patterns associated with different phylogenetic groups. Ann. Bot. **119:** 1021–1033.

Verhertbruggen, Y., Marcus, S.E., Haeger, A., Ordaz-Ortiz, J.J., and Knox, J.P. (2009). An extended set of monoclonal antibodies to pectic homogalacturonan. Carbohydr. Res. **344:** 1858–1862.

Vincken, J.P., Schols, H.A., Oomen, R.J., McCann, M.C., Ulvskov, P., Voragen, A.G., and Visser, R.G. (2003). If homogalacturonan were a side chain of rhamnogalacturonan I. Implications for cell wall architecture. Plant Physiol. **132:** 1781–1789.

Willats, W.G., Limberg, G., Buchholt, H.C., van Alebeek, G.J., Benen, J., Christensen, T.M., Visser, J., Voragen, A., Mikkelsen, J.D., and Knox, J.P. (2000). Analysis of pectic epitopes recognised by hybridoma and phage display monoclonal antibodies using defined oligosaccharides, polysaccharides, and enzymatic degradation. Carbohydr. Res. **327:** 309–320.

Woolfenden, H.C., Bourdais, G., Kopischke, M., Miedes, E., Molina, A., Robatzek, S., and Morris, R.J. (2017). A computational approach for inferring the cell wall properties that govern guard cell dynamics. Plant J. **92:** 5–18.

Xiao, C., Barnes, W.J., Zamil, M.S., Yi, H., Puri, V.M., and Anderson, C.T. (2017). Activation tagging of Arabidopsis POLYGALACTURONASE INVOLVED IN EXPANSION2 promotes hypocotyl elongation, leaf expansion, stem lignification, mechanical stiffening, and lodging. Plant J. **89:** 1159–1173.

Xiao, C., Somerville, C., and Anderson, C.T. (2014). POLYGALACTURONASE INVOLVED IN EXPANSION1 functions in cell elongation and flower development in Arabidopsis. Plant Cell **26:** 1018–1035.

Yang, Y., Costa, A., Leonhardt, N., Siegel, R.S., and Schroeder, J.I. (2008). Isolation of a strong Arabidopsis guard cell promoter and its potential as a research tool. Plant Methods **4:** 6.

Zablackis, E., Huang, J., Müller, B., Darvill, A.G., and Albersheim, P. (1995). Characterization of the cell-wall polysaccharides of *Arabidopsis thaliana* leaves. Plant Physiol. **107:** 1129–1138.

Zhao, L., and Sack, F.D. (1999). Ultrastructure of stomatal development in Arabidopsis (Brassicaceae) leaves. Am. J. Bot. **86:** 929–939.